Breaking bending limit of large-diameter thin-walled aluminum alloy tube considering cryogenic effects on material properties and friction behaviors

Hong Sun [a,b], Heng Li [a,*], Heng Yang [a,b], Yang Liu [a], Xuancheng Hao [a], Riming Cong [a], Hao Guan [a], M.W. Fu [b,#]

[a] State Key Laboratory of Solidification Processing, School of Materials Science and Engineering, Northwestern Polytechnical University, Xi'an, 710072, China

[b] Department of Mechanical Engineering, The Hong Kong Polytechnic University, Hung Hom, Kowloon, Hong Kong, China

[*,#] Corresponding authors. [*]Email: liheng@nwpu.edu.cn, [#] Email: mmmwfu@polyu.edu.hk

Abstract

The large-diameter thin-walled (LDTW) aluminum alloy (Al-alloy) tubes with small bending radius have been widely used in the aerospace field due to the superiority in terms of high transmission efficiency, high spatial margin and weight reduction. However, it is a tough issue to deform a desirable bent tube with such extreme specification since induced heavier nonuniform deformation may cause tension and compression instabilities such as overthinning, cracking and wrinkling. Considering possible enhancement in mechanical properties of Al-alloy when deformed at cryogenic temperature (CT), the cryogenic bending potential of the Al-alloy tubular materials is to be excavated. In this work, bending temperature was set at room temperature (RT), -60℃, -120℃, and -180℃. Under cryogenic condition, properties of fracture energy C, anisotropy index r, strength factor K and hardening index n are all improved and friction coefficients between tube and tooling dies show varying degrees of reduction. A finite element model considering material anisotropy at CT was conducted and an innovative cryogenic bending involving internal and external cooling was designed. It is proved that tube formability evaluated by bending defects of wall thinning and wrinkling can be effectively improved by cryogenic bending. As the temperature decreases, tube thickness reduction decreases continuously, however, the degree of wrinkling decreases first and then increases, and the most optimum temperature was obtained at -60℃. For wall thinning, cryogenic enhancement of C, r and n can reduce it, conversely, a larger K at CT intensifies it. The decreasing in friction of wiper die and pressure die at CT can promote wall thinning but only to a very small extent. For wrinkling, the opposite effects of strength factor K and hardening index n mainly cause of the non-monotonic relation between the temperature and wrinkling degree. The friction of bending die also has an impact to increase wrinkling at CT. Bending limit has been further explored and it has been improved from R_d=3.0D at RT to 1.0D at -60℃. Cryogenic bending of LDTW Al-alloy tubes with R_d=2.0D at -60℃ was finally experimentally performed. The results of cryogenic bending successfully verified the effect of cryogenic temperature on developing formability of LDTW Al-alloy tubes.

Keywords

Bending limit, LDTW Al-alloy tube, Cryogenic material properties, Cryogenic friction behavior.

Highlights

- Mechanical properties are overall improved at cryogenic temperature, the opposite effects of strength factor K and hardening index n mainly cause of the non-monotonic relation between the temperature and wrinkling degree.
- The friction coefficients between tube and tooling dies exhibit varying degrees of decline at cryogenic temperature, which have less impacts on tube formability.
- An innovative cryogenic bending involving internal and external cooling was designed and an accurate finite element model was established and verified.
- Bending limit has been improved from 3.0D bending radius at room temperature to 1.0D at -60°C, and it was confirmed for tubes with 2.0D bending radius experimentally by cryogenic bending.

1 Introduction

Aluminum alloy (Al-alloy) tubes have been widely used in pipeline systems of aerospace, aviation, navigation, automobile and other manufacturing fields due to its advantages of light weight, high formability, as well as good corrosion resistance [1]. Large-diameter thin-walled (LDTW) Al-alloy bent tubes with outer diameter-to-thickness ratios more than 20 ($D/t > 20$), small-bending radius ($R_d < 2.0D$, R_d is the bending radius) and high transmission efficiency are required in harsh service conditions like aerospace fuel transportation and environmental control systems[2],[3]. The extreme specifications of the tube have a series priority in service environment, however, it brings great difficulties to its forming and manufacturing [4]. Various forming defects such as wrinkling, thickness reduction and even cracking [5] will occur, and restraint the increase in forming limit, as shown in Fig. 1. The tube outer bending ridgeline is mainly subjected to biaxial tensile stress state in axial and circumferential directions, and inner ridgeline is subjected to biaxial compressive stress state, correspondingly to forming defects of wall thinning and wrinkling, respectively [6]. Therefore, tube bending limit is measured by the minimum bending radius that can be achieved by the standard limited by forming defects. It is a tough issue to obtain a desirable bent tubular part with extreme specification of large diameter, thin wall, and small bending radius.

Fig. 1. Bending defects of cracking and wrinkling of LDTW tubes.

There have been some efforts to achieve promising formability of the hard-to-form tubes. For bending of rectangular H96 tube, a flexible PVC mandrel was proposed by Zhu et. al [7] and it was found that it leads to a smaller tube thickness variation and a more uniform tube thickness distribution compared with the traditional mandrel-cores, for the PVC mandrel brings about smaller stress in the bending process. Liu et. al [8] also took the flexible PVC material as the groove fillers in the bending process of H-typed double-ridged rectangular tube, and successfully improved tube bending quality. Although the flexible mandrel can provide flexible support, the process of taking out the mandrel after bending requires heating and melting, and it is difficult to remove the mandrel for large-angle bending tubes. In the past decade, heating-assisted bending has been employed to improve bending formability of LDTW tubes owing to the developed ductility and reduced deformation resistance at elevated temperatures [9],[10]. Zhang et al. [11] and Tao et al. [12] improved bending quality of LDTW commercial pure titanium alloy CP-Ti tubes by the developed the warming bending technology. Simonetto et al. [13] developed the direct hot rotary draw bending (DHRDB) for processing 22MnB5 hollow profiles process and confirmed that DHRDB can effectively increase bending accuracy and nearly absent springback. Furthermore, Yang et al. [2] designed a differential heating-based rotary draw bending method to proactively coordinate the non-uniform deformation, and forming quality of the LDTW titanium tube was effectively enhanced. The method of warm bending to improve tube quality and bending limit is more suitable for titanium and steel tubes that have high temperature stability. For aluminum alloys especially thin-walled components, however, it is easy to be oxidized at high temperature and material performance will be changed after oxidation, which will affect its later service. So warm bending is not suitable for LDTW Al-alloy tubes.

In recent years, Al-alloy materials have been found to exhibit remarkable enhancement of strength and ductility simultaneously when deformed at cryogenic temperature (CT) [14],[15], which provides great potential to improve the forming performance of Al-alloy components by cryogenic forming. Fan et al. [16] solved the coexistence of wrinkling and splitting of Al-alloy thin shell by a forming process at ultra-low temperature gradient. Yuan et al. [17] proposed a novel deep drawing process at CT of Al-alloy sheets and found that the deep drawability was significantly enhanced as the temperature decreased to -160 °C. Schneider et al. [18] carried out a limiting dome height drawing test of EN AW-5182 and EN AW-6016 alloys at low temperatures and explored that the stretch formability can be enhanced obviously at temperatures below 25℃. Liu et al. [19] studied the formability and flow stress of an Al-Cu-Mn alloy sheet under biaxial stress state at various CT and quantified that the formability and deformation uniformity of the sheet at CT were considerably increased. Sotirov et al. [20] provided optimum forming technology for manufacturing complex aluminum body panels, and cryogenic forming method was proved to offer a higher forming limit for deep drawing of complex sheet products of work hardening 5xxx Al-alloy sheets. The cryogenic forming of Al-alloy is also beneficial to reduce or eliminate residual

stress. A novel cryogenic treatment proposed by Araghchi et al. [21] can relieve up to 71% of the residual stresses in 2024 Al-alloy at -196℃ compared to 29% related to the traditional treatment. However, the cryogenic bending potential of LDTW Al-alloy tubes still remain unknown.

Based on the above, it can be reasonably speculated that cryogenic forming also has great potential to reduce bending defects and improve formability of the hard-to-bend Al-alloy tubes. However, cryogenic bending for LDTW Al-alloy tubes presents new challenges. On the one hand, LDTW tubes tend to be anisotropic, which affects the plastic deformation, and consequently, their forming limits [22]. Material anisotropy is also affected by cryogenic conditions [23], but it is very difficult to accurately characterize [24], [25]. So, accurate charactering the anisotropy of the thin-walled tubes at CT become a crucial issue to explore the cryogenic bending potential of LDTW Al-alloy tubes [26], [27]. On the other hand, tube bending is conducted under complex constraints [6], bending quality of LDTW tubes is also significantly influenced by multiple friction behaviors between tubes and various tooling dies [28]. While the friction behavior is also affected by cryogenic condition [29], which makes the effect of CT on tube bending formability more complicated and uncertain. Therefore, the roles of the two key factors mentioned above, viz. anisotropic mechanical properties of the tubes and friction behaviors between tube and tooling dies, are studied in this work to explore the cryogenic formability and improve bending limit.

In this research, taking the cryogenic bending of LDTW (D/t=89) 6061-O tubes as the research object, deformation temperature was set to -60℃, -120℃ and -180℃, respectively. As a comparison, the tube bending under RT was also conducted. Bending limit is represented by the minimum R_d that the tube can achieve under the condition of meeting the forming quality requirements of no wrinkle and thickness reduction rate within 25%. First, cryogenic characterization of material anisotropy and friction behavior was carried out. An integrated characterization method combined uniaxial tension test and VPSC-based simulation was used to determine the plastic anisotropy at CT. Then, the modeling of rotary draw bending process of LDTW Al-alloy tubes was conducted and validated. Next, a cryogenic bending platform was designed and the cooling efficiency was determined. Based on above, cryogenic bending potential of LDTW 6061-O Al-alloy tubes was evaluated by wrinkling and tube wall thinning. Inhibition mechanism of CT on bending defects has been explored from aspects of mechanical properties and friction behaviors. Bending limit of such LDTW Al-alloy tube is finally improved at CT, and cryogenic bending was successfully performed. An overall research framework is given in Fig. 2.

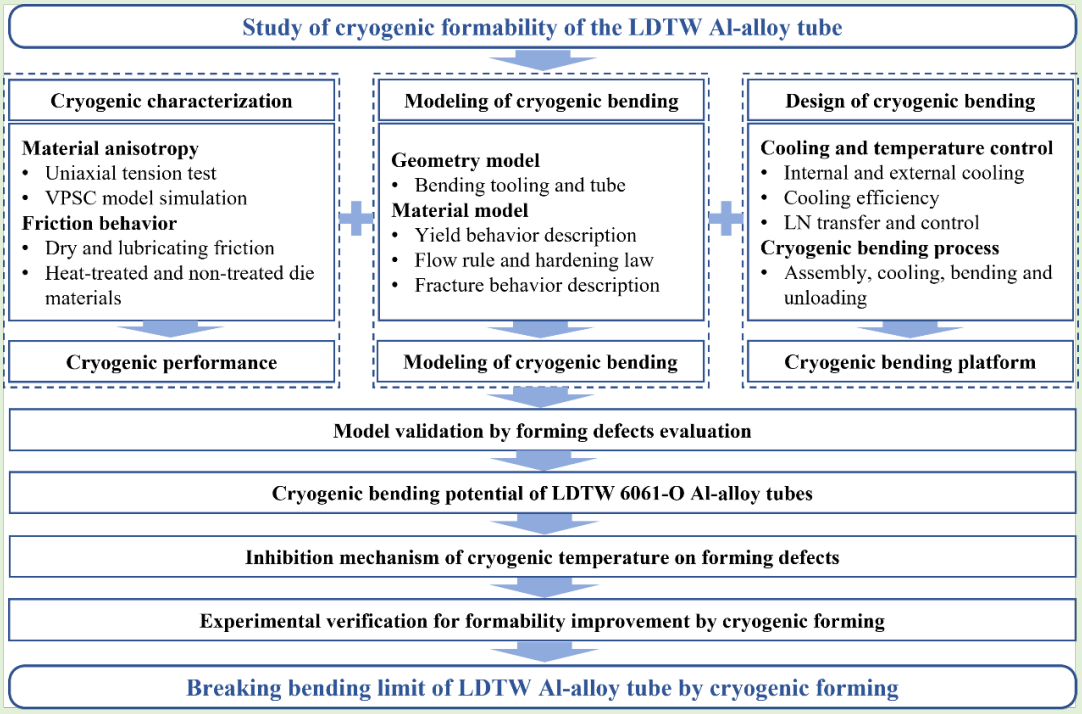

Fig. 2. Research framework.

2 Material anisotropy and friction at cryogenic temperature

The as-received material is LDTW 6061-O Al-alloy tubes with the fully annealed state based on the standard of SAE AMS-WW-T-700/6. The tubes are with specifications of 63.5 mm in diameter and 0.71 mm in wall thickness (D/t=89). The main chemical composition of the material is given in Table 1.

Table 1. The main chemical composition of 6061-O Al-alloy tubes.

Element	Si	Fe	Cu	Mn	Mg	Cr	Zn	Ti	Al
Content (%)	0.80	0.70	0.40	0.15	1.20	0.35	0.25	0.15	remainder

The anisotropy and friction of the material are very critical to the bending formability of LDTW tubes, while these properties are often temperature sensitive. Therefore, the accurate characterization of these key parameters is very important cryogenic forming of LDTW tubes. In this section, an integrated characterization method was approached to determine material anisotropy at CT and a friction test was inducted to obtain the cryogenic friction properties.

2.1 Integrated characterization of mechanical properties at cryogenic temperature

- *Design of integrated characterization*

An integrated characterization method comprising of uniaxial tension test and VPSC model were used to determine mechanical properties and plastic anisotropy of the tubes at CT and RT.

The anisotropy index r-value and yield strength σ of uniaxial tension in 0º, 45º and

90º directions and balanced biaxial tension (BBT) at RT and CT are distinguished by subscript as r_0, r_{45}, r_{90}, r_b, σ_0, σ_{45}, σ_{90}, and σ_b, which are required in solving parameters of material constitutive model. The r-value is defined as the ratio of transverse strain ε_x and thickness strain ε_z, as expressed in Eq. (1).

$$r = \left| \frac{\varepsilon_x}{\varepsilon_z} \right| \tag{1}$$

The specimens and collets of uniaxial tension in 0º, 45º and 90º directions were designed and made [30], as shown in Fig. 3.

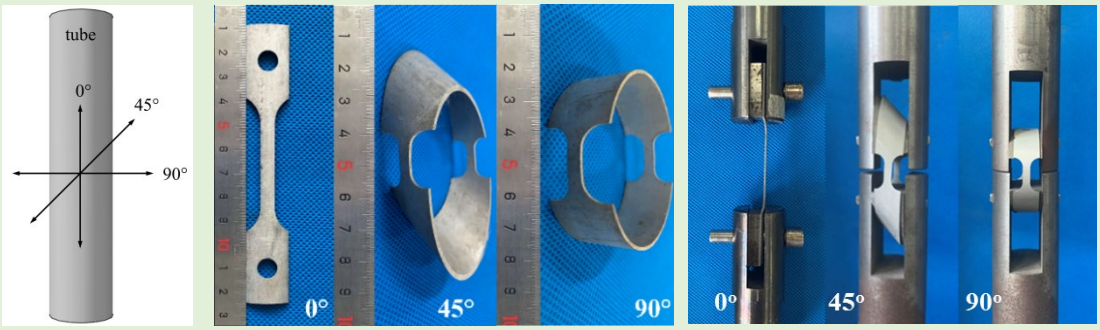

(a) (b) (c)

Fig. 3. The specimens and collets of axial tension at 0º, 45º and 90º directions: (a) axial tension directions, (b) the specimens, (c) the collets with specimens.

The tests were conducted on an electronic universal testing machine equipped an insulated cabinet with a temperature-controlled system, as shown in Fig. 4. The temperature control accuracy of the insulation system is 3°C. The test temperature was set to RT, -60°C, -120°C and -180°C, respectively. The cryogenic test environment was realized by connecting liquid nitrogen (LN) and temperature control system. The nominal strain rate is 0.001 s^{-1}, which is consistent with the tube bending. Each set under the same conditions was repeated at least three times to reduce errors. All specimens were stretched to failure.

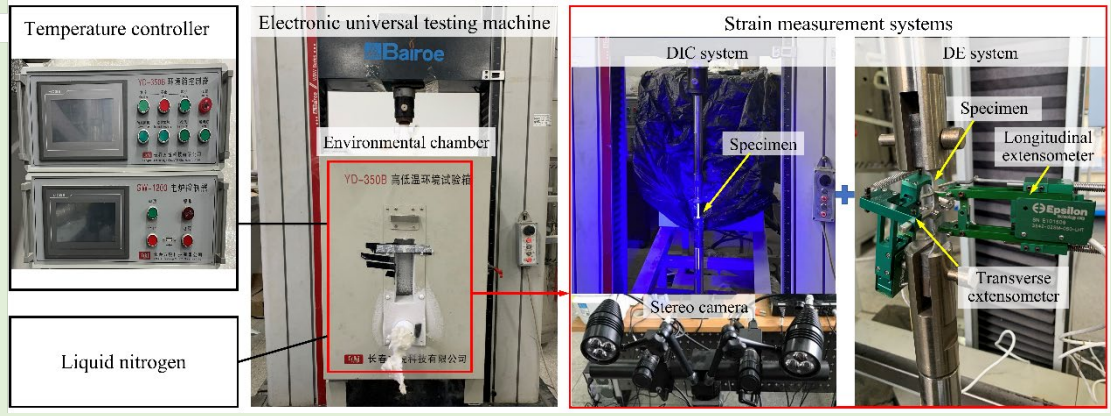

Fig. 4. Experimental platform of cryogenic tension test consisting of an electronic universal testing machine equipped an environment chamber and strain measurement systems of DIC system and DE system.

To obtain r-values in tension test, longitudinal strain along the tension direction and transverse strain vertical to the tension direction of the specimen have to be measured

at the same time. Two kinds of strain measurement systems were employed in different conditions for their own advantages and limitations. One is a digital image correlation (DIC) system, and another one is a dual extensometer (DE) system consisting of a longitudinal extensometer and a transverse extensometer. Since the DIC system does not directly contact the specimen during measurement, it does not have much requirements on the geometry of the specimen, which is every suitable for the hoop tension specimen. But it is only applicable for testing at RT, as the limitation in measuring cryogenic deformation for the nature of speckle paint that is easy to fall off at cryogenic temperature. Therefore, the DE system was used for its convenience of cryogenic measurement, while it was limited in 45º and 90º tension tests for the closed hoop geometry that restricted the clamp of the two extensometers. In this way, the tension tests in all different directions at RT were tested by DIC system and those in 0º direction at whether RT or CT were measured by DE system.

For the anisotropic parameters that are difficult to be determined by experiment methods in this study, namely r_{45}, r_{90} at CT and BBT at RT and CT, the VPSC-based simulation was adopted. VPSC model accounts for full anisotropy in properties and response of the single crystals and the aggregate [31]. It simulates the plastic deformation of aggregates subjected to external strains and stresses. VPSC is based on the physical shear mechanisms of slip and twinning, and accounts for grain interaction effects. In addition to providing the macroscopic stress-strain response, it accounts for hardening, reorientation and shape change of individual grains. As a consequence, it predicts the evolution of hardening and texture associated with plastic forming. The simulation procedure was applied to deformation of the LDTW 6061-O Al-alloy tubes.

Fundamentally it is characterized by an evolution of the threshold stress with accumulated shear strain in each grain of the form in Eq. (2), associated with slip (or twinning) system s [32].

$$\hat{\tau}^{s} = \tau_0^{s} + (\tau_1^{s} + \theta_1^{s}\Gamma)(1 - \exp(-\Gamma\left|\frac{\theta_0^{s}}{\tau_1^{s}}\right|)) \tag{2}$$

where Γ is the accumulated shear strain in the grain which can be expressed in Eq. (3).

$$\Gamma = \sum_{s} \Delta\gamma^{s} \tag{3}$$

where γ^{s} is the local shear-rate on slip system (s), τ_0, θ_0, θ_1, (τ_0+τ_1) are the initial critical resolved shear stress (CRSS), the initial hardening rate, the asymptotic hardening rate and the back-extrapolated CRSS. In addition to self-hardening, each slip system also has an interactive hardening effect. The interactive hardening effect can be expressed by Eq. (4),

$$\Delta\tau^{s} = \frac{d\hat{\tau}^{s}}{d\Gamma}\sum_{s'} h^{ss'}\Delta\gamma^{s'} \tag{4}$$

where $\Delta\gamma^{s'}$ is the increase in the threshold stress of a system due to shear activity, $h^{ss'}$ is the coupling coefficient, and the $\Delta\tau^{s}$ is the CRSS increment related to shear activity. In addition, defining the coupling coefficients $h^{ss'}$ has capability of 'self' and 'latent' hardening in the model, and empirically accounts for the obstacles that new dislocations associated with s' activity represent for the propagation of system s.

The deformation mechanism considered is <111>{110} slip system and <111>{112} twinning system for Al-alloy tubes in this research. The key parameters that have to resolve in VPSC model related to the two deformation mechanisms include τ_0, τ_1, θ_0, and θ_1, which determine the CRSS and hardening behavior during deformation. Here self-hardening is used as a reference and set coupling coefficients $h^{ss'}$=1 [32], and the evolution of the threshold stress is given by only the Voce hardening function in Eq. (5).

$$\Delta\tau^s = \frac{d\hat{\tau}^s}{d\Gamma}\Delta\Gamma \tag{5}$$

The data obtained by the experiment provides reliable basis for the establishment and validation of the VPSC model, and the simulation can just make up for the incapability in the experimental methods. The characterization method used in each deformation condition is listed in Table 2.

Table 2. The characterization method used in each deformation condition.

Temperature	RT				CT			
Deformation	0º	45º	90º	BBT	0º	45º	90º	BBT
Method	DIC/DE	DIC	DIC	VPSC	DE	VPSC	VPSC	VPSC

- *Uniaxial deformation in 0° at RT and CT*

Fig. 5 gives the true stress-strain curves obtained by 0º uniaxial tension tests at RT and CT. The mechanical properties are listed in Table 3. It can be found that with the temperature decreasing, the mechanical properties have enhanced significantly. Compared with the mechanical properties at RT, the ultimate strength and elongation at -180℃ has improved 89.6% and 33.9% respectively, which provides the basis and prerequisite for the subsequent cryogenic forming. It can be obtained from Fig. 5 (b) that LDTW 6061-O Al-alloy tubes have a significant anisotropy behavior when tension in different directions.

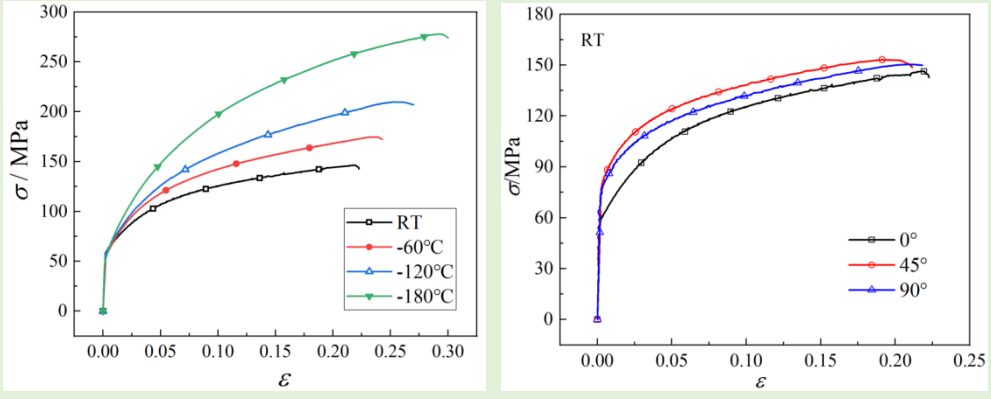

(a) (b)

Fig. 5. True stress-strain curves obtained by uniaxial tension tests: (a) 0° tension at different temperatures, (b) 0°, 45° and 90° tension at RT.

Table 3. Mechanical properties of 6061-O Al-alloy tubes of 0º tension at RT and CT.

Mechanical properties	RT	-60℃	-120℃	-180℃
Elastic modulus E/GPa	29.3	32.6	34.6	35.1
Yield strength σ_y/MPa	57.2	57.5	58.8	59.1
Strength factor K/MPa	211.4	257.9	332.8	445.7
Elongation δ/%	22.1	24.0	26.2	29.6
Ultimate strength σ_m/MPa	146.2	174.6	209.6	277.2
Hardening index n	0.23	0.26	0.33	0.36
Anisotropic index r_0	0.57	0.67	0.76	0.87
Fracture energy C/kJ•m^{-3}	26.9	34.1	44.1	63.4

- *VPSC-based simulation for BBT and uniaxial deformation in 45° and 90° directions at CT*

The VPSC model of Al-alloy tubes was established and validated based on experiment results. A total of 1779 crystal orientations from the EBSD result were used in the VPSC model to explore the plastic anisotropy. The stress-strain curves from the experiment of uniaxial tension along 0° tension at RT and CT was used as the input data for solving model parameters. Based on the genetic algorithm in MATLAB, the model parameters related to slip and twinning systems in VPSC model were determined, and the VPSC model of the 6061-O Al-alloy tubes at RT and CT was obtained.

For VPSC modeling, an electron backscatter diffraction (EBSD) testing was performed on Al-alloy tubes. The microstructure of the initial specimen and deformed specimen after tension in 0° direction at RT and -180 ℃ is obtained, both deformed at 0.2 nominal strain. The obtained microstructure is shown in Fig. 6.

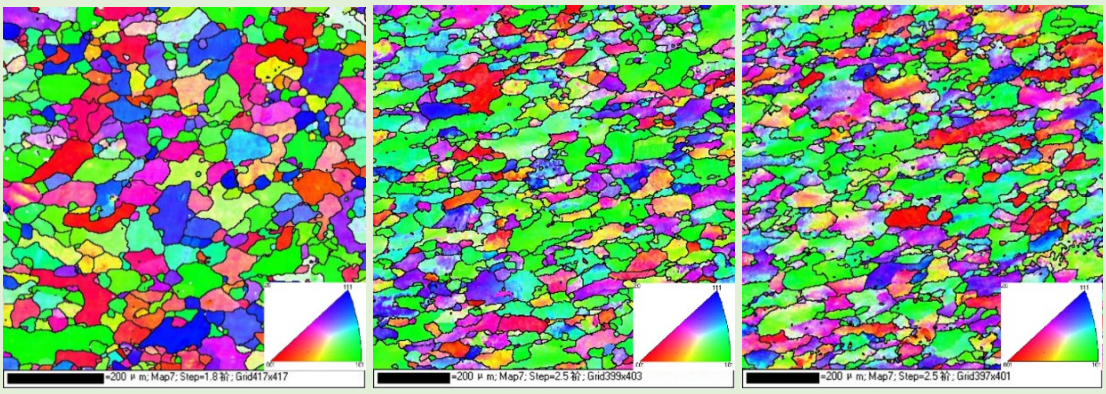

(a) (b) (c)

Fig. 6. Microstructure of 6061-O Al-alloy tubes: (a) undeformed initial specimen, (b) deformed at 0.2 nominal strain at RT and (c) deformed at 0.2 nominal strain at -180℃.

Based on the results of material microstructure and stress-strain data, the key parameters related to slip and twinning systems of LDTW 6061-O Al-alloy tubes in VPSC model have been solved, as given in Table 4.

Table 4. The solved parameters for VPSC model.

Temperature	Deformation mechanism	τ_0 /MPa	τ_1 /MPa	θ_0 / MPa	θ_1 / MPa
RT	SLIP <111>{110}	30	29	491	26
	TWIN <111>{112}	839	42	714	329
-60℃	SLIP <111>{110}	30	38	510	35
	TWIN <111>{112}	834	52	716	329
-120℃	SLIP <111>{110}	31	45	542	47
	TWIN <111>{112}	834	54	716	329
-180℃	SLIP <111>{110}	34	64	600	60
	TWIN <111>{112}	842	52	714	329

It can be seen from Table 4 that the four parameters τ_0, τ_1, θ_0, θ_1 of the dislocation slip deformation mechanism all increase with the decrease of temperature, that is, the CRSS and strain hardening in the deformation process increase with the decrease of temperature, which is consistent with the obtained results of mechanical properties. While the parameters related to twinning deformation under different temperature conditions are almost unchanged, indicating that the twinning mechanism does not play a dominant role under low temperature conditions, which is consistent with the results shown in Fig. 6. Therefore, the enhancement mechanism of the mechanical properties at cryogenic temperature is considered as the higher initial CRSS and strengthen of dislocation slip.

The plastic deformation stage of stress-strain curves obtained by tests and the texture of deformed specimens was taken to validate the calibrated VPSC model. The tension curves and *r*-values are compared with the corresponding VPSC-based simulation results in Fig. 7. It can be found that the simulation results have a high degree coincidence with the experimental ones. By quantitatively analysis, the maximum error between the simulation and experiment results are explored. The errors of the stress-strain curves fitted by VPSC-based simulation are all within 6% compared to the experiment results. The *r*-values predicted by the model are overall a little higher than the experimental value, while the errors of the solved *r*-values are within 10%. Therefore, the established VPSC model of LDTW Al-alloy tubes is validated, and it can be quantitatively considered reliable.

A further validation of the established VPSC model is by predicting texture evolution of 606-O Al-alloy tube. The pole figures obtained by EBSD test and VPSC-based simulation are proposed in Fig. 8 to make comparison. The texture results are taken from the 0° tension at RT and -180℃ when the deformation strain is 0.2. The result shows that brass and copper texture occur during the tension deformation, and the VPSC model is also quite accurate in predicting the texture evolution of 6061-O Al-alloy tubes during tensile deformation.

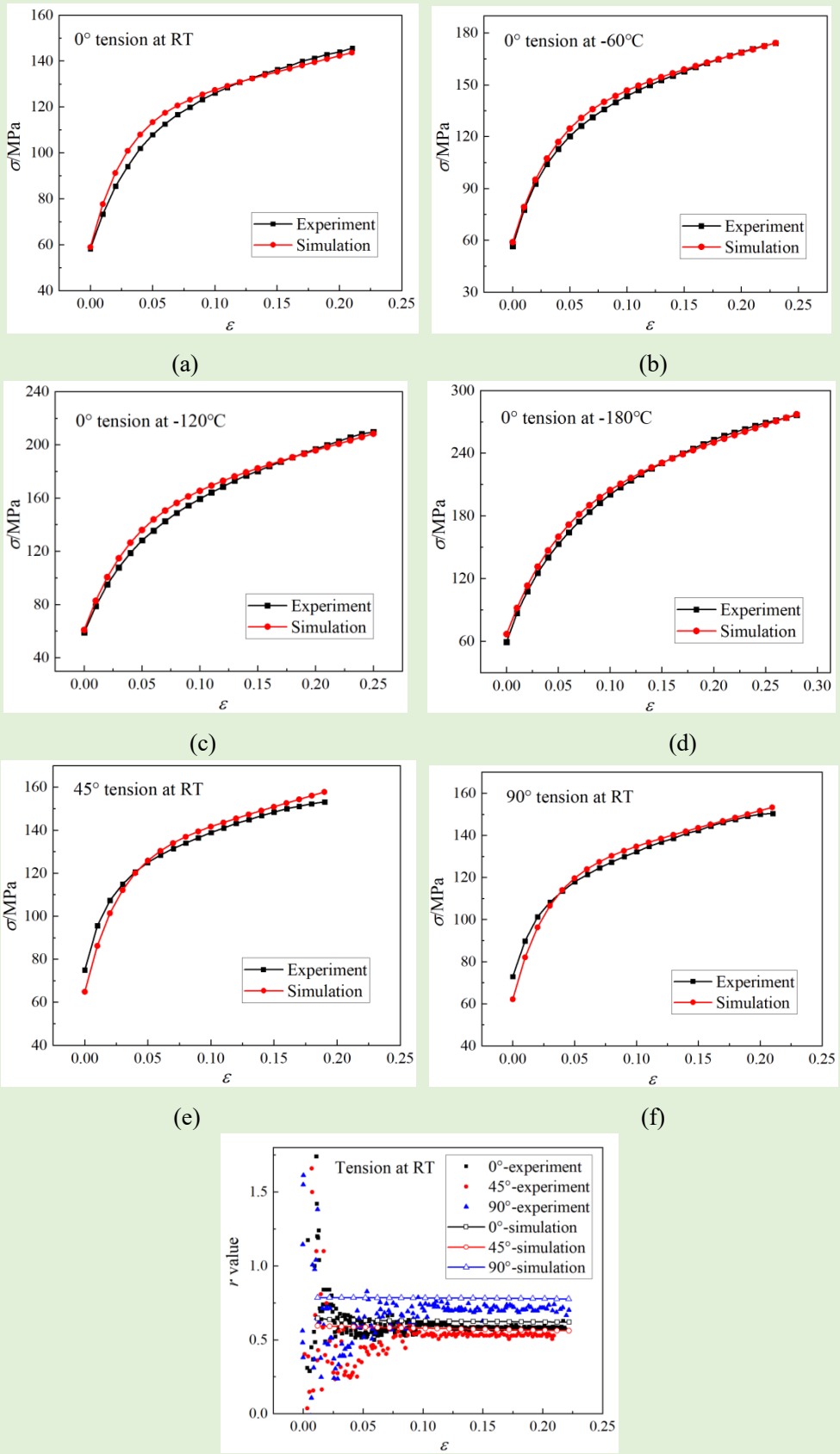

Fig. 7. VPSC-based simulation and experiment results: stress-strain curves of 0° tension at (a) RT, (b) -60°C, (c) -120°C, (d) -180°C, stress-strain curves of (e) 45° and (f) 90° tension at RT, and (g) *r* values of different directions at RT.

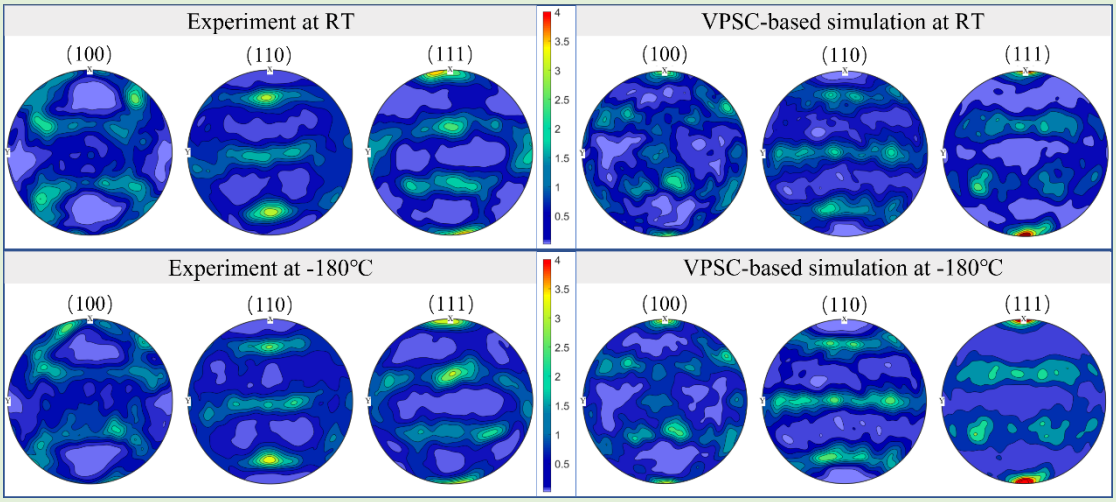

Fig. 8. The pole figures taken from the sample of 0° tension at RT and -180°C when the deformation strain is 0.2.

Based on the validation of the above two aspects, it can be proved that the established VPSC model is reliable and can be applied for simulation of the material parameters that are difficult to obtain in experiments.

The key mechanical parameters required to further calibrate the constitutive modeling include yield strength and *r*-value, so far have been obtained by experiments and VPSC model simulation, which are given in Table 5. In the table, σ refers to the yield strength, and subscript refers to tension direction and BBT state, respectively.

Table 5. Parameters for 6061-O Al-alloy tubes cryogenic modeling.

Temperature	σ_{y0}/MPa	σ_{y45}/MPa	σ_{y90}/MPa	σ_{yb}/MPa	r_0	r_{45}	r_{90}	r_b
RT	57.2	63.1	62.2	56.8	0.57	0.53	0.71	1.46
-60°C	57.5	64.9	62.2	58.8	0.67	0.63	0.80	1.47
-120°C	58.8	67.0	64.3	60.8	0.76	0.68	0.82	1.46
-180°C	59.1	73.5	70.5	66.6	0.87	0.71	0.83	1.45

2.2 Friction at cryogenic temperature

A cryogenic friction test was conducted to obtain the friction coefficients of different contact pairs between tubes and tooling dies. In this test, MMU-5G friction testing machine equipped a temperature controller was used to determine the friction coefficient between 6061-O Al-alloy tubes as the sample below and tooling die material Cr5Mo1V as the sample on top at RT and CT, as shown in Fig. 9 (a). The testing chamber is connected to LN to realize cryogenic environment. In the cryogenic environment, the lubricating oil commonly used at normal temperature is no longer suitable. Polytetrafluoroethylene (PTFE) polymer has self-lubrication and temperature stability, so a PTFE spray lubricant with an applicable temperature range of -180°C to 200°C was used as lubricant for cryogenic friction condition, as shown in Fig. 9 (b).

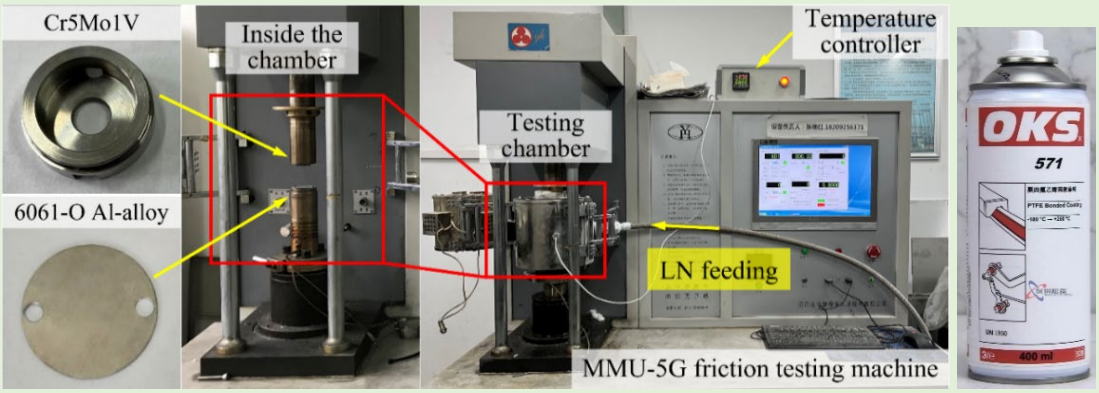

(a) (b)

Fig. 9. Cryogenic friction testing platform: (a) schematic diagram of MMU-5G friction testing machine and friction torsion test platform inside testing chamber, (b) PTFE spray lubricant.

According to the actual friction conditions in tube bending experiment, the friction conditions were set as dry friction and lubricating friction at RT and CT, respectively. Except for wiper die, the die materials adopt the heat treatment process of nitriding and sandblasting. So, the tooling die materials contains the heat-treated die materials for pressure die, bending die, clamping dies and mandrel die, and non-treated die materials for wiper die. The friction condition that between the tube and pressure die, clamping die is dry friction, while the friction between the tube and wiper die, bending die and mandrel is under lubricating conditions. The results of the friction coefficients are given in Fig. 10 and Table 6, and the friction coefficient is obtained from the average value of the stable section of each friction curve.

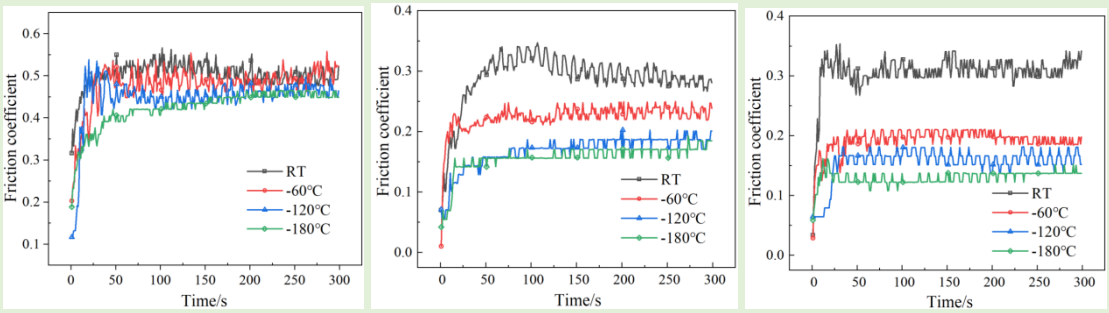

(a) (b) (c)

Fig. 10. Friction coefficients between 6061-O Al-alloy tubes and (a) heat-treated Cr5Mo1V die materials under dry friction condition, (b) heat-treated Cr5Mo1V die materials under lubricating condition and (c) non-treated Cr5Mo1V die materials under lubricating condition.

Table 6. Friction test conditions.

Friction condition	Contact pair	Temperature	Friction coefficient μ
Dry friction	6061-O Al-alloy tubes and heat-treated Cr5Mo1V die materials	RT	0.51±0.02
		-60°C	0.48±0.02
		-120°C	0.46±0.02
		-180°C	0.45±0.02

Lubricating	6061-O Al-alloy tubes and heat-treated Cr5Mo1V die materials	RT	0.29±0.02
		-60℃	0.23±0.01
		-120℃	0.19±0.02
		-180℃	0.17±0.02
Lubricating	6061-O Al-alloy tubes and non-treated Cr5Mo1V die materials	RT	0.31±0.02
		-60℃	0.20±0.01
		-120℃	0.17±0.01
		-180℃	0.13±0.01

It can be found from the results that cryogenic temperature does affect friction coefficients. As the temperature getting lower, the friction coefficients all decrease. The friction coefficient of 6061-O Al-alloy tubes and heat-treated Cr5Mo1V die materials under dry friction condition decreases slightly, while that of the other two friction test under lubricating condition decreases significantly. This is attributed to two aspects, one is the sensitivity of the material itself to cryogenic temperature, and the other is the sensitivity of the lubricant to temperature, both of which lead to the decrease of friction coefficients with cryogenic temperature, which also explains the reduction of friction coefficient under dry friction conditions is not as dramatically as that under lubricating conditions. As one of the important bending forming parameters, friction coefficient will also affect the tube formability in cryogenic bending.

3 Modeling of tube rotary draw bending at cryogenic temperature

Due to the complexity and high cost of the cryogenic bending experiment, numerical simulations were used to explore the formability of Al-alloy tubes at CT and RT. The cryogenic forming of the LDTW tubes involves multiple nonlinearities in material, geometry, and stress state, that is, strong anisotropy of materials, thin-walled thickness and small bending radius, and complex stress states in the forming process. For the cryogenic condition, the key issues of geometry and technical characteristics of the cryogenic bending were set reasonably. Furthermore, the accuracy of anisotropic constitutive model and friction behavior at CT are very critical to the reliability of the FE model. Based on the material properties characterized at CT and RT in Section 2, the anisotropic plasticity and friction behaviors in cryogenic bending were reasonably considered in modeling. Finally, a FE model of the tube rotary draw bending at RT and CT was established.

3.1 Geometric model

The geometric model includes a tube, a pressure die, a couple of clamping dies, a wiper die, a bending die and a mandrel. The tube is set as a deformable body, and all molds are set as rigid bodies. The bending radius is equal to twice the tube diameter, and the bending angle is set as 90°. Since the Al-alloy tube is a LDTW part, the geometric model of the tube is simplified to a shell that ignores the thickness-direction

stress. Since the FE model of the LDTW tube bending is symmetrical with respect to the bending neutral layer, a half-model is adopted to improve the calculation efficiency, and symmetry boundary constraint has to be set on the bending neutral layer. The established geometry model is shown in Fig. 11.

During the rotary draw bending process, there are complex contacts, including the interfaces between the tube and the molds. The mold with high rigidity is taken as the primary surface, while the tube is set to the secondary surface. The penalty function is used to define the contact constraints and the friction behavior between the contact pairs is described by the Coulomb friction model. The friction coefficients are reasonably set for each friction condition, referring to Table 6.

Based on the ABAQUS/Explicit platform, the cryogenic rotary draw bending model has been established as shown in Fig. 11.

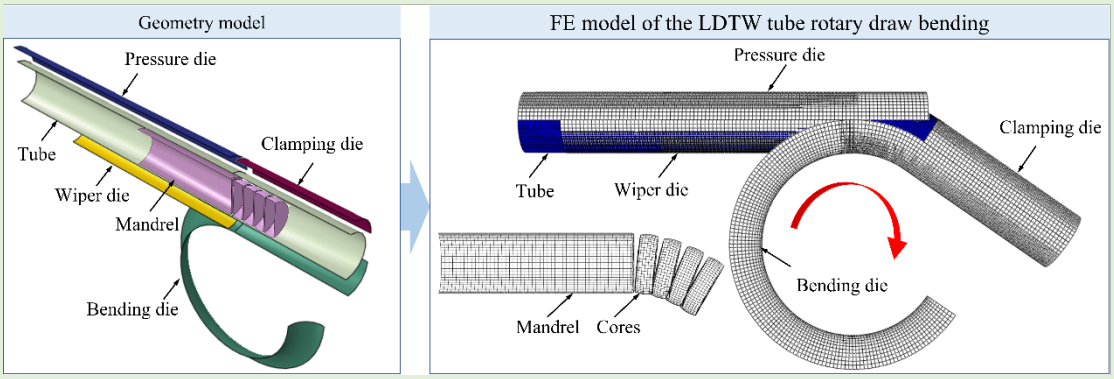

Fig. 11. FE model of rotary draw bending of the LDTW Al-alloy tubes.

3.2 Material model

- *Yield behavior description*

As an important part of material constitutive, the yield criterion has a great influence on the prediction accuracy of FE simulation. The cryogenic forming of the tube involves multiple nonlinearities in material, geometry, and stress state, that is, strong anisotropy of materials, thin-walled thickness and small bending radius, and complex stress states in the forming process. For such extremely tough issue, the yield criterion employment becomes more critical [33].

Two kinds of anisotropic yield criteria, namely Hill'48 [34] and YLD2000-2D, have been selected to describe the material yield behavior. In the FE simulation study on the bending forming of the extremely thin-walled tube, the thickness-direction stress of the tube is ignored during the bending forming, and the stress state is simplified to the plane stress state.

Hill'48 criterion in plane stress state is expressed as Eq. (6), where parameters F, G, H, N can be determined by r_0, r_{45} and r_{90}, as expressed in Eq. (7).

$$f = (G+H)\sigma_1^{\,2} + (F+H)\sigma_2^{\,2} - 2H\sigma_1\sigma_2 + 2N\sigma_{12}^{\,2} - \bar{\sigma}^2 = 0 \tag{6}$$

$$\begin{cases} F = \dfrac{r_0}{r_{90}(r_0+1)} \\ G = \dfrac{1}{r_0+1} \\ H = \dfrac{r_0}{r_0+1} \\ N = \dfrac{(r_0+r_{90})(2r_{45}+1)}{2r_{90}(r_0+1)} \end{cases} \tag{7}$$

The anisotropic yield criteria YLD2000-2D, containing anisotropic parameters related to various deformation conditions, have been widely applied to describe the yield behavior of Al-alloy material with strong anisotropic plasticity [35]. In the FE simulation study on the bending forming of the extremely thin-walled tubes, the thickness-direction stress of the tube is ignored during the bending forming, and the stress state is simplified to the plane stress state. YLD2000-2D anisotropic yield function adopts a linear transformation mathematically which divides the yield function into two parts and introduces 8 parameters to solve the function. The yield function that reduces to the function proposed by Hershey [36] and Hosford [37] can be simply expressed in Eq. (6),

$$\phi = \phi'(X') + \phi''(X'') = 2\bar{\sigma}^a \tag{6}$$

where,

$$\phi' = \left|X'_1 - X'_2\right|^a \tag{7}$$

$$\phi'' = \left|X''_1 + 2X''_2\right|^a + \left|X''_2 + 2X''_1\right|^a \tag{8}$$

In the equations, ϕ' and ϕ'' are two anisotropic functions according to the two principal states for the plane stress state and they are obtained by linear transformation of the stress tensor matrix [35].

The material correlation parameters included in the YLD2000-2D yield criterion are eight linear conversion coefficients α_1 to α_8 and crystallographic constant m. For FCC Al-alloy materials, m is equal to 8. The linear conversion coefficients require the corresponding eight materials mechanical parameters solved above, viz., the yield strength and thickness anisotropy index of axial tension in 0°, 45°, 90° directions and the BBT state respectively.

The linear conversion coefficients α_1 to α_6 are related to the normal stress, which are obtained by substituting the stress state, yield strength and thickness anisotropy index of the axial tension in 0°, 90° directions and the BBT state obtained in Table 5 into the Eq. (9) which satisfies the yield strength and Eq. (10) which satisfies r value respectively, then six octave equations will be obtained, and the values of coefficients α_1 to α_6 can be solved. In the Eqs (9) and (10), γ, δ, q_x and q_y have been calculated and determined by Barlat [35], and $\bar{\sigma}$ is the effective stress.

$$F = \left|\alpha_1\gamma - \alpha_2\delta\right|^a + \left|\alpha_3\gamma - \alpha_4\delta\right|^a + \left|\alpha_5\gamma - \alpha_6\delta\right|^a - 2\left(\frac{\bar{\sigma}}{\sigma}\right)^a = 0 \tag{9}$$

$$G = q_x \frac{\partial \phi}{\partial s_{xx}} - q_y \frac{\partial \phi}{\partial s_{yy}} = 0 \tag{10}$$

The linear conversion coefficients α_7 and α_8 are coefficients related to shear stress state. The stress state of tension in the 45° direction is decomposed to the shear stress in the axial and circumferential directions of the tube. Therefore, the yield strength and the thickness anisotropy index of tension in 45° are used to substitute into the Eqs. (11) and (12), and two more octave equations are obtained. By combining the above eight octave equations, the eight linear conversion coefficients α_1 to α_8 of the YLD 2000-2D yield criterion can be solved.

$$F = \left|\frac{\sqrt{k_2^{'2} + 4\alpha_7^2}}{2}\right|^a + \left|\frac{3k_1'' - \sqrt{k_2''^2 + 4\alpha_8^2}}{4}\right|^a + \left|\frac{3k_1'' + \sqrt{k_2''^2 + 4\alpha_8^2}}{4}\right|^a - 2\left(\frac{\bar{\sigma}}{\sigma_{45}}\right)^a = 0 \tag{11}$$

$$G = \frac{\partial \phi}{\partial \sigma_{xx}} + \frac{\partial \phi}{\partial \sigma_{yy}} - \frac{2a\bar{\sigma}^a}{\sigma(1 + r_{45})} = 0 \tag{12}$$

where,

$$k_2^{'} = \frac{\alpha_1 - \alpha_2}{3} \tag{13}$$

$$k_1'' = \frac{2\alpha_5 + \alpha_6 + \alpha_3 + 2\alpha_4}{9} \tag{14}$$

$$k_2'' = \frac{2\alpha_5 + \alpha_6 - \alpha_3 - 2\alpha_4}{3} \tag{15}$$

The function parameters of the two yield criteria for 6061-O Al-alloy tube at different temperatures have been solved based on the material characterization. The coefficients are given in Table 7.

Table 7. Yield function parameters of 6061-O tube cryogenic deformation.

Criterion	Temperature	F	G	H	N				
Hill'48	RT	0.511	0.637	0.363	1.183				
	-60℃	0.476	0.599	0.401	1.243				
	-120℃	0.527	0.568	0.432	1.292				
	-180℃	0.561	0.535	0.465	1.325				
Criterion	Temperature	α_1	α_2	α_3	α_4	α_5	α_6	α_7	α_8
YLD 2000-2D	RT	0.967	0.887	1.179	0.989	0.991	0.839	0.876	0.859
	-60℃	0.997	0.854	1.090	0.959	0.969	0.764	0.852	0.816
	-120℃	1.031	0.845	1.093	0.964	0.968	0.796	0.863	0.816
	-180℃	1.142	0.660	1.002	0.891	0.922	0.638	0.787	0.735

Correspondingly, deformation yield locus of the tubes at different temperatures are proposed, as illustrated in Fig. 12. As the deformation temperature decreases, the yield locus gradually expands outward, and it explains the improvement in yield strength of

the 6061-O Al-alloy tubes at CT. YLD2000 yield criterion not only considers the uniaxial stress state of uniaxial tension, but also introduces the biaxial stress state, while Hill'48 criterion only involves parameters describing uniaxial stress state.

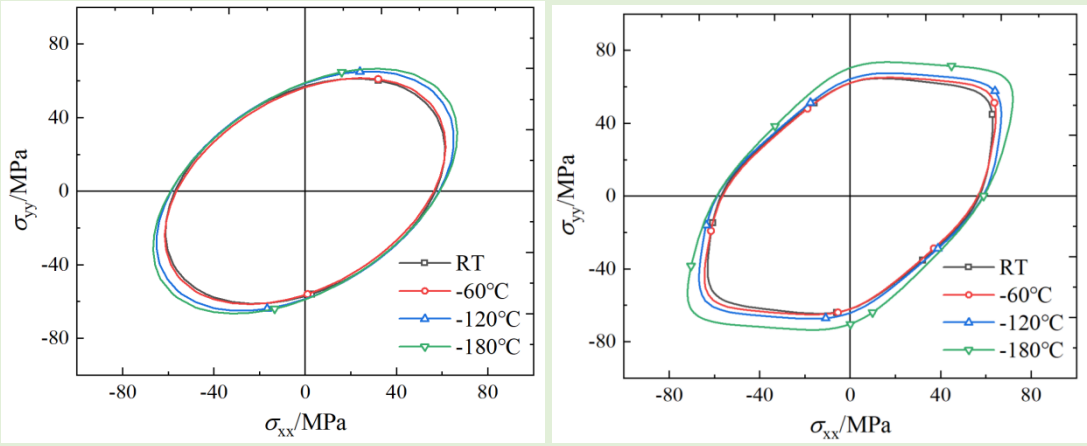

Fig. 12. Yield loci of LDTW Al-alloy tubes at different temperatures by different yield criterions: (a) Hill'48, (b) YLD2000-2D.

- *Fracture behavior description*

Since there is a certain risk of fracture in the LDTW tube bending, the fracture criterion is used to predict the materials failure. The uncoupled ductile fracture criteria have been used widely due to its simple formulation and ease of calibration [38]. In the uncoupled approach, damage accumulation is formulated empirically or semiempirically with the general function in terms of certain macroscopic variables, such as the equivalent plastic strain, principal stress, shear stress, and hydrostatic stress, all of which capture fracture initiation and propagation [39]. The uncoupled fracture criterion employed in this study was designated in Eq. (18),

$$\int_0^{\bar{\varepsilon}_f} \bar{\sigma} \mathbf{d}\bar{\varepsilon}^p = C \tag{18}$$

where $\bar{\varepsilon}_f$ is the equivalent plastic strain to fracture, $\bar{\sigma}$ is the equivalent stress, $\bar{\varepsilon}^p$ is the equivalent plastic strain. C is the threshold fracture energy of materials. The plasticity and fracture data of uniaxial tension were used to determine the C value at CT and RT. The values of C at different temperatures were determined by the total plastic work at the critical point of fracture, which were obtained in Table 3.

In addition, a FE model of 0º axial tension test employed YLD2000-2D yield criterion was established to verify the fracture model, and the stress-strain curves of simulation and experiment results are compared, as shown in Fig. 13. The maximum relative error of the simulation is within 6%, which can be considered that the material model is reliable.

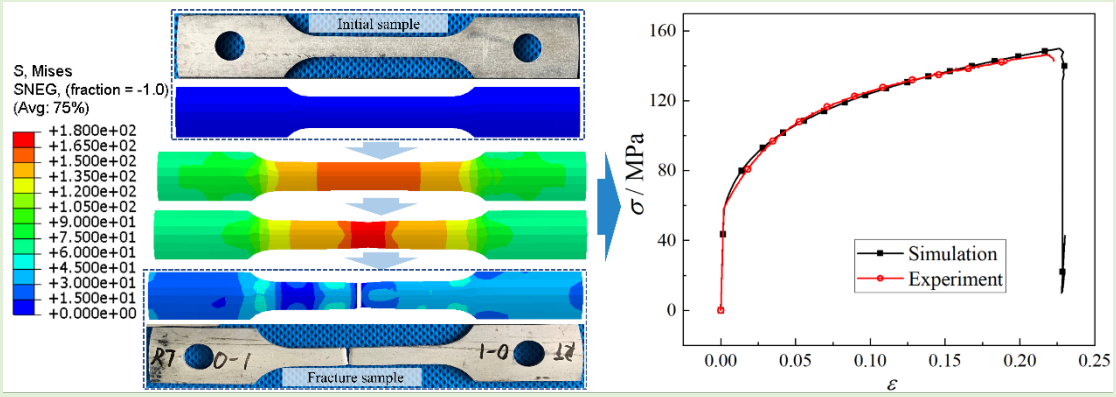

Fig. 13. Fracture model validation: FE model simulation result of 0º tension and a comparison of stress-strain curves of simulation and experiment results.

4 Design of tube rotary draw bending at cryogenic temperature

As a typical forming process of bending tubes, rotary draw bending method [5] has the characteristics of high efficiency, good quality, easy control, and high precision, which is an appropriate chosen for LDTW tube bending studied in this work. A computer numerical control (CNC) tube bender was used in this bending experiment platform to realize tube rotary draw bending, and the tooling for rotary draw bending contains a pressure die, a wiper die, a bending die, a couple of clamping dies, and a mandrel with several mandrel balls.

Due to the cryogenic forming potential of Al-alloy materials, a cryogenic bending platform of LDTW Al-alloy tubes was designed. Compared with bending forming at RT, the difficulty of cryogenic bending experiment mainly lies in how to realize the cooling, temperature measurement and temperature control of the tubes in an unenclosed space.

4.1 Cooling and temperature control system

The operating environment of tube rotary draw bending is open and cannot be sealed, therefore, the key to cryogenic bending lies in regional cooling and temperature maintenance. Since the deformation of tube rotary draw bending is at the bending tangent point, it is very critical to focus cooling and temperature control on bending tangent point and its surrounding area during deformation process.

It is designed two kinds of cooling channels to realize tube cooling during the whole bending process, namely internal and external cooling of tube. The internal cooling is feeding LN directly into the inside of tube. A plug with appropriate size, as shown in Fig. 14 (a), was fixed at the end of the tube to reduce the circulation between the tube inner space and the outside environment and maximize the internal cooling efficiency. When LN delivery is opened, it will flow into the tube continuously through the channel connected to the plug, and the tube can be cooled from the inner.

The external cooling of the tube is realized by tooling structure design. During the bending process, the area of tube bending tangent point is always in contact with the forming molds of pressure die and wiper die. Due to the thin wall of tubes and the high thermal conductivity of Al-alloy materials, cooling the mold can conduct the tube to be

cooled from the outside. Uniform cooling channels connecting LN were designed on the pressure die and wiper die, as shown in the Fig. 14 (b), which can ensure efficient and uniform cooling the area around the bending tangent point.

Additionally, temperature monitor and control are also very critical to cryogenic environment maintenance. Two monitor points were selected to obtain the temperatures at inner and outer sides of tube tangent point, respectively. The outer monitor point is at the front end of the pressure die contacting tube outer surface and the inner one is at the first mandrel ball contacting tube inner surface. A thermometer connected to a couple of thermocouples was used and two induction contacts with bimetallic strain gauges of the thermocouples were placed at the two monitor points to record temperatures. LN was connected to the internal and external cooling channels and its flow velocity can be controlled by valve regulation to cool down and maintain temperature. The cryogenic experiment platform of tube rotary draw bending was finally conducted, as shown in Fig. 14 (c).

To determine the cooling efficiency of internal and external cooling channels respectively, the cooling effects of three cooling modes are investigated and compared, namely only external cooling, only internal cooling, and both internal and external cooling. The time taken to reach the target CT from RT under different cooling modes was measured to determine cooling efficiency, and the results are shown in Table 8. It indicates that the internal and external cooling mode has the shortest cooling time and the highest cooling efficiency and can achieve a cooling of -180 °C within half an hour. For the cooling of inner monitor point, it takes about the same time for internal cooling and external cooling, while for the cooling of outer monitor point, the cooling efficiency of external cooling is higher than that of internal cooling. Both monitor points need to reach the target temperature, so the cooling time is determined to be the longest of the two monitor points. In this way, the efficiency of only external cooling and only internal cooling is almost the same. In addition, when the external cooling method is used, the temperature of the outer monitor point is always lowered faster than that of the internal monitoring point. This is because the pressure die contacting the outer monitor point has a deeper cooling channel than the wiper die contacting the inner monitor point due to geometry, which makes the temperature lower down faster. Therefore, considering the cooling efficiency corresponding to different target temperatures, it is very necessary to cool down the tube by dual cooling of inner and outer channels.

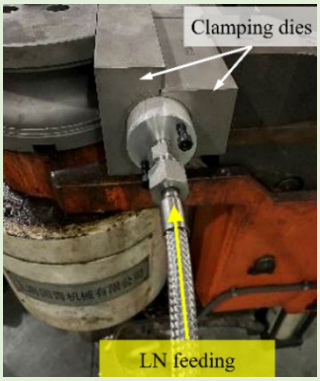

(a)

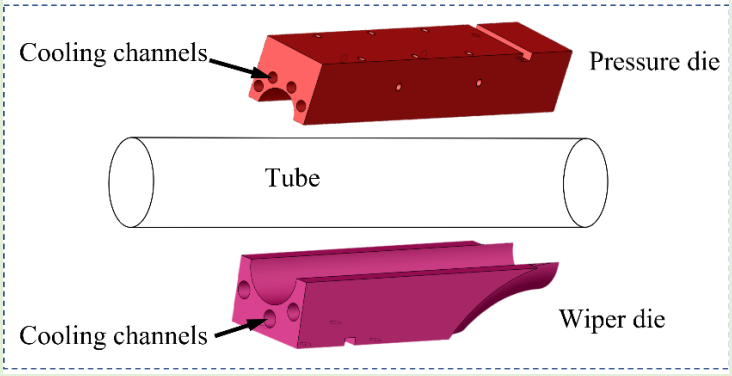

(b)

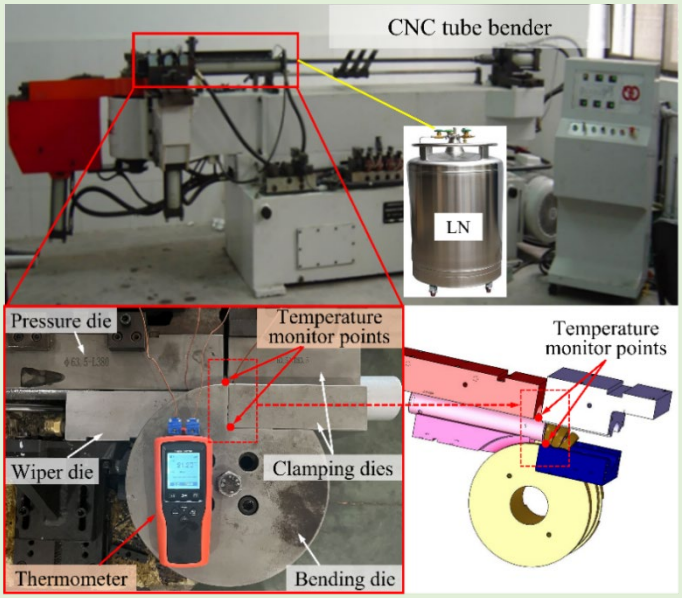

(c)

Fig. 14. Design of tube rotary draw bending at cryogenic temperature: (a) internal cooling, (b) external cooling, (c) temperature monitor and control of the cryogenic experiment platform of tube rotary draw bending.

Table 8. The cooling time taken from RT to the target temperature by different cooling modes.

Target temperature	Monitor point	Time of external cooling	Time of internal cooling	Time of internal and external cooling
-60℃	Inner	12 mins	12 mins	7 mins
	Outer	7 mins	12 mins	5 mins
-120℃	Inner	29 mins	28 mins	18 mins
	Outer	21 mins	26 mins	11 mins
-180℃	Inner	＞ 30 mins	＞ 30 mins	28 mins
	Outer	＞ 30 mins	＞ 30 mins	19 mins

4.2 Cryogenic bending process

Based on the established cryogenic experiment platform of tube rotary draw bending, a set of experimental procedures consisting of four parts was also designed, as shown in Fig. 15.

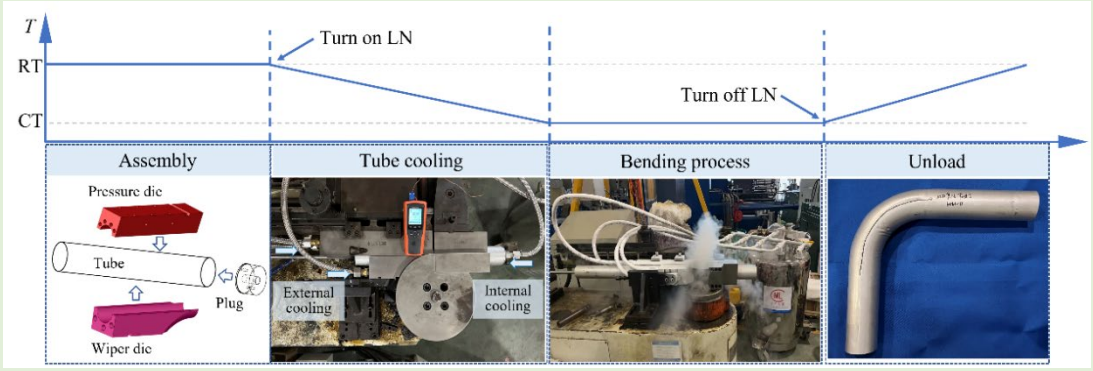

Fig. 15. Experimental procedures of cryogenic bending process.

The first step is assembly of tube and tooling. Firstly, fix a thermocouple on the inner monitor point, and put the tube on the mandrel. Then, assemble wiper die, bending die, pressure die and a couple of clamping dies in sequence, followed by placing another thermocouple at the outer monitor point. Next, the plug for internal cooling was assembled to the end of tube. Finally, the preparation was done by connecting LN delivery pipes to the cooling channels on the plug and forming dies.

The second step is to cool down the tube. Turn on the thermometer and check if it works normally. Next, turn on the internal and external cooling systems, LN can be continuously fed in cooling channels, and the temperature near the bending tangent point begins to drop. When it drops to the required temperature, it can be controlled by adjusting the flow velocity of LN. When the temperature has stabilized at the desired temperature, the bending test can begin.

The third step is tube bending forming. First the bending parameters has to be set to CNC system of the tube bender. The angular velocity is 1°/s and set the feed speed of pressure die according to tube radius and bending radius. The bending angle in this work is set to 90°. Start the CNC bender to bend the tube to the setting angle, and temperature needs to be monitored and controlled during the whole bending process.

The last step is to close the LN delivery and unload all tooling constrains to remove the tube. Finally, the bent tube sample can be obtained by such experimental procedures of cryogenic bending.

5 Results and discussions

5.1 Model validation by bending defects evaluation

The forming quality and bending limit of LDTW tubes are restricted by various defects. In order to quantitatively evaluate tube formability, an evaluation method shown in Fig. 16 (a) was approached in this work. The bending center is taken as the origin point, the distance from each point along the bending inner ridge to the origin point is measured, signified the distance as L. Due to the different bending radii, the distance H of the bent tubes with different bending radii is also different. For the convenience of comparison, subtract the corresponding bending radius R_d from the H value, then adding half time of the tube diameter D to this value, which defined as W, as illustrated in Eq. (19). Then, the curve obtained by W corresponding to bending angle α of every point is taken as wrinkle indication, so the inner ridgeline curve of the tubes with different bending radii can be compared.

$$H = L - R_\mathrm{d} + 0.5D \tag{19}$$

Defined the average distance from the wrinkle peak to the troughs on both sides as the wave height of a wrinkle, as ΔH given in Eq. (20), where H_p is the height of the wrinkle peak and H_{t1} and H_{t2} are the heights of the wrinkle troughs on both sides, respectively. Wall thinning of the outer ridge is evaluated by wall thickness reduction rate Δt of every point along the outer ridgeline, as defined as Eq. (21), where t is the initial wall thickness, and t' is the tube wall thickness after bending.

$$\Delta H = H_p - \frac{1}{2}(H_{t_1} + H_{t_2}) \tag{20}$$

$$\Delta t = \frac{|t - t'|}{t} \times 100\% \tag{21}$$

The evaluation indicators as described above can be easily obtained by the visualization of FE model for simulation results. The wrinkling produced by actual tube bending, however, is relatively difficult to accurately measure by ordinary vernier calipers and screw micrometers. Therefore, a three-dimensional (3D) scanning equipment, named AltaScan handheld laser 3D scanner shown in Fig. 16 (b), is used to accurately measure the wrinkling defects for experiment results. The tube wall thickness data was collected by cutting and measuring the bent tubes every 10°, as shown in Fig. 16 (c).

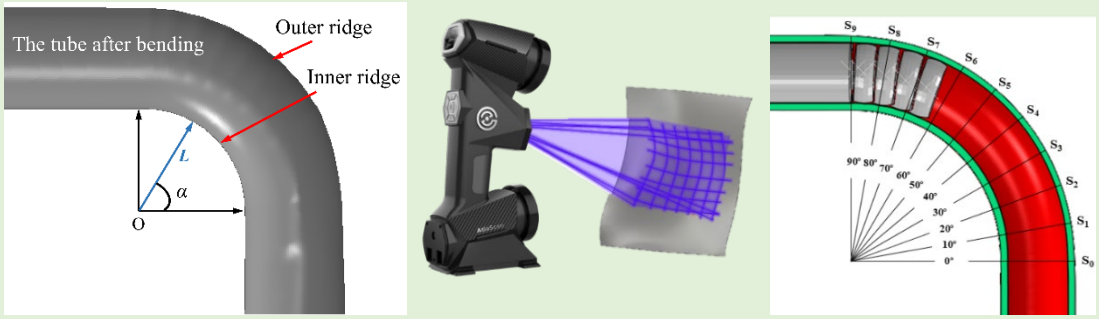

(a) (b) (c)

Fig. 16. Indicators and measurement method of defects evaluation: (a) schematic diagram of defect evaluation of tube after 90° bending, (b) 3D scanner for wrinkling measurement in experiment results, (c) schematic diagram of tube cross-section cuttings for thickness measurement in experiment results.

Experiments of rotary draw bending of the LDTW tube with $R_d = 2.0D$ at RT and -60°C were carried out to validate the model. Fig. 17 shows the sample bent at RT and a comparison with the simulation results by the two yield criteria. It can be seen that the bent sample at RT is significantly wrinkled, and there are cracks at the severe wrinkles. Obviously, YLD2000 yield criterion can more accurately describe the wrinkling and crack than the Hill'48 criterion. The essential reason should be explained from the nonlinear stress state of the thin-walled tube during bending process. The key stress states of biaxial tension and biaxial compression for tube bending are developed in YLD2000 criterion, which is the fundamental reason why it is better than Hill'48 in predicting the formability. Thus, YLD2000-2D criterion was employed to describe the yield behavior of tube bending.

Forming defects are quantitatively measured and compared, as shown in Fig. 18. For the tube bent at RT, the average ΔH of simulation result and experiment result is 1.18 mm and 1.13 mm respectively, and the relative error is 4.2%. The average Δt of simulation result and experiment result is 0.163 and 0.148 respectively, and the relative error is 9.2%. For cryogenic bending at -60°C, the average ΔH of simulation result and experiment result is 0.22 mm and 0.21 mm respectively, and the relative error is 4.5%, and the absolute error is only 0.01 mm which is very small. The average Δt of simulation result and experiment result is 0.124 and 0.113 respectively, and the relative error is

9.7%, the absolute error is only 0.012. Thus, it can be considered that the established FE model for rotary draw bending of LDTW 6061-O Al-alloy tubes is accurate and reliable.

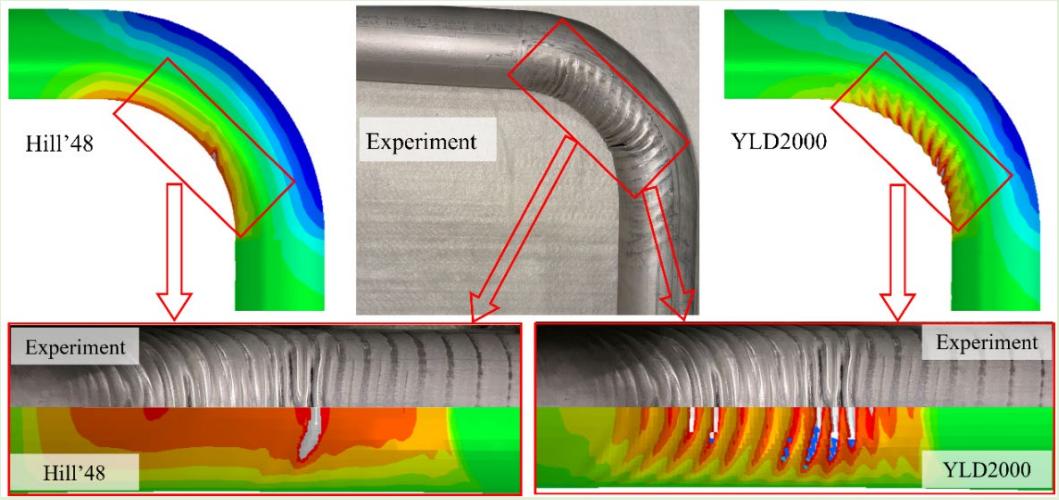

Fig. 17. Bending experiment result at RT with 2.0*D* bending radius and a comparison of wrinkling patterns with simulation results by the two yield criteria.

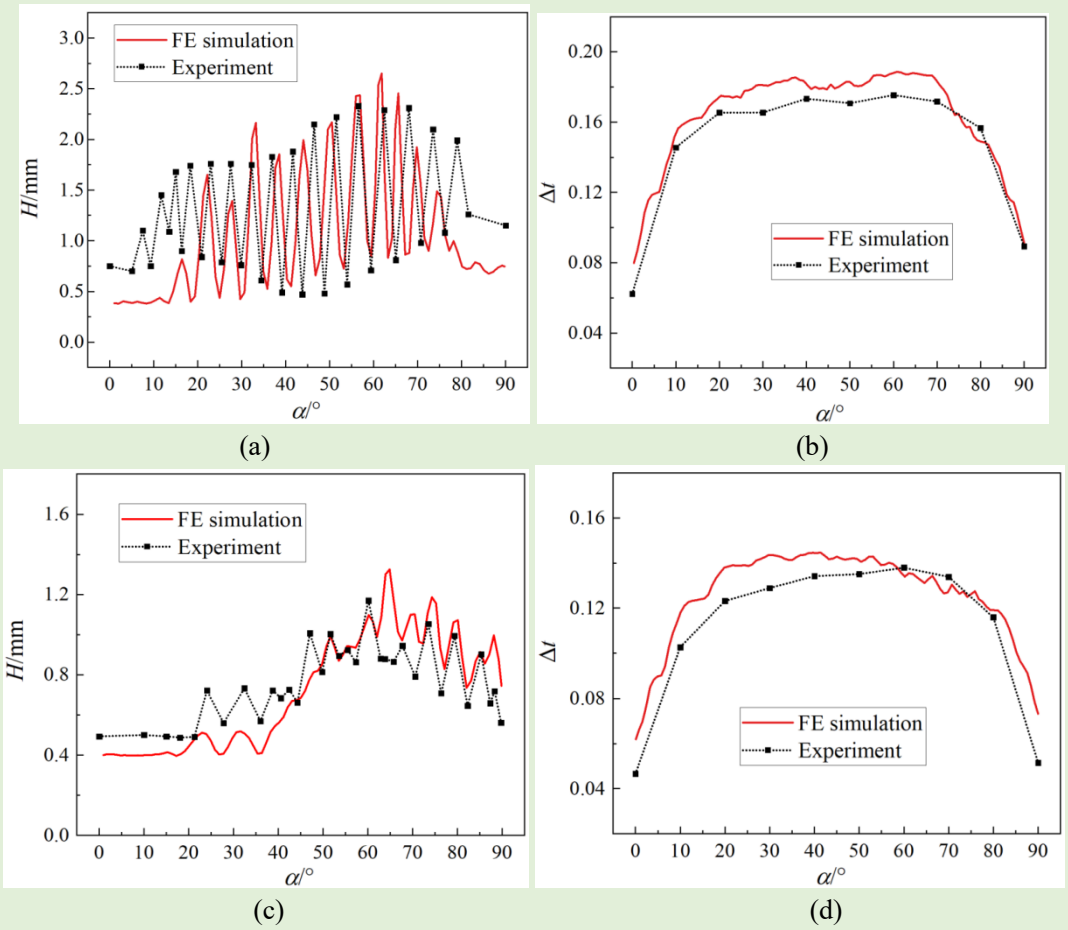

Fig. 18. Results of forming defects with 2.0*D* bending radius by simulation and experiment: (a) wrinkling pattern along tube inner ridgeline at RT, (b) wall thickness reduction rate along tube outer ridgeline at RT, (c) wrinkling pattern along tube inner ridgeline at -60℃ and (d) wall thickness reduction rate along tube outer ridgeline at -60℃.

5.2 Cryogenic bending potential of LDTW 6061-O Al-alloy tubes

- *Tube formability at RT*

Bending radius was set as 3.0*D* and 2.0*D* to explore the tube formability bending at RT, and the results are shown in Fig. 19. It can be seen from the figure that when the bending radius is 3.0*D*, the bending forming quality at RT is good. There is no wrinkle on the inner ridge, and the thinning rate on the outer ridge does not exceed 12%. However, when bending radius is improved to 2.0*D*, the wall thickness reduction rate is still within 25%, while the inner ridge is obviously wrinkled, and cracks appears in the wrinkle valleys. Therefore, the bending limit of LDTW 6061-O Al-alloy tubes at RT is 3.0*D*.

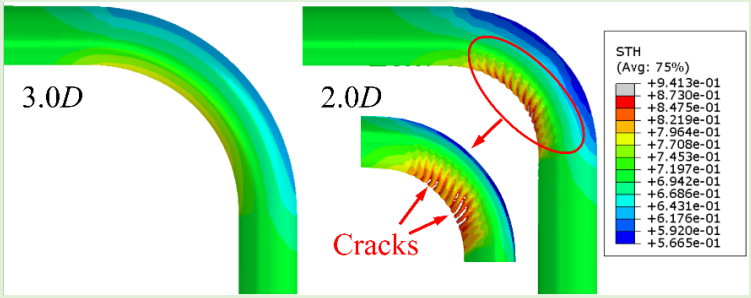

(a)

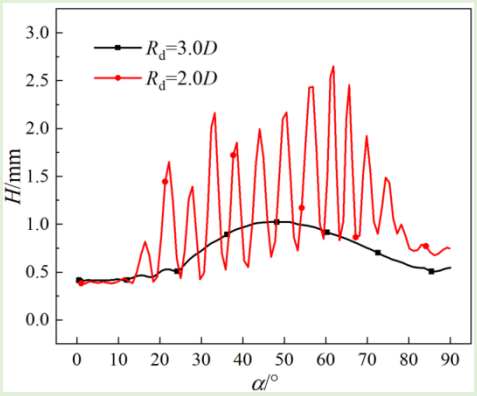

(b)

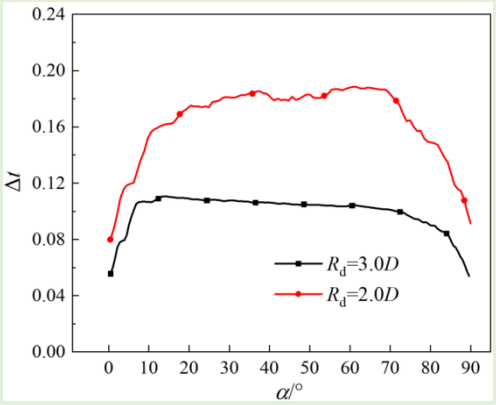

(c)

Fig. 19. Results of rotary draw bending of LDTW 6061-O Al-alloy tubes with 3.0*D* and 2.0*D* bending radii at RT: (a) overview of simulation results, (b) wrinkling pattern along tube inner ridgeline, (c) wall thickness reduction rate along tube outer ridgeline.

- *Tube formability at CT*

Considering that the forming quality is poor when the bending radius is 2.0*D* at RT, the bending process of tubes with 2.0*D* bending radius was performed at CT by simulations to explore the cryogenic bending potential of LDTW 6061-O Al-alloy tubes.

The simulation results of the tube after bending 90° at CT are shown in Fig. 20, and wrinkling curves and thickness reduction rate were quantitatively characterized, which are given in Table 9. When the wave height exceeds half time of the wall thickness, that is 0.35 mm, it is counted as a wrinkle wave. Although there are some waves whose wave height does not exceed 0.35 mm in Fig. 20 (b), it is only considered that there is a tendency to wrinkle in these places, yet not a real wrinkle.

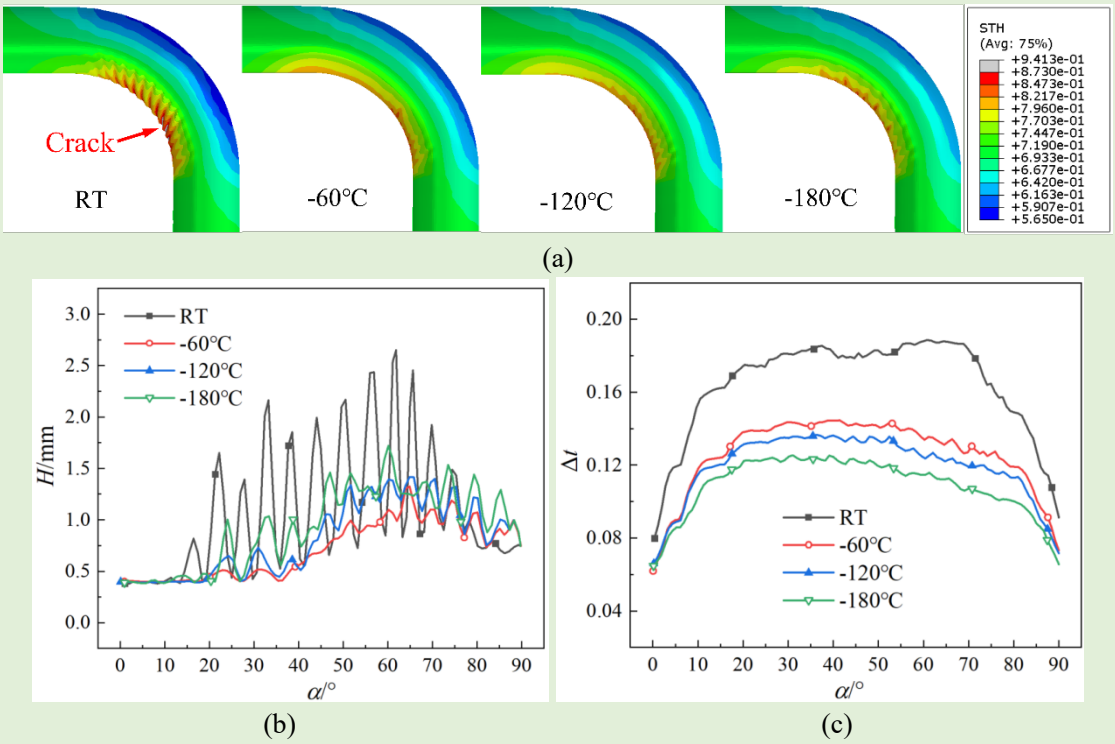

Fig. 20. Results of rotary draw bending of LDTW 6061-O Al-alloy tubes with 2.0*D* bending radius at RT and CT: (a) overview of simulation results, (b) wrinkling pattern along tube inner ridgeline, (c) wall thickness reduction rate along tube outer ridgeline.

Table 9. Forming defects at different temperatures.

Temperature	Number of $\Delta H >$ 0.35 mm	Average ΔH /mm	Maximum ΔH /mm	Average Δt	Maximum Δt
RT	12	1.18	1.81	0.164	0.189
-60°C	0	0.22	0.35	0.125	0.144
-120°C	3	0.28	0.41	0.119	0.136
-180°C	7	0.43	0.60	0.109	0.125

It can be found that cracks appeared only when the tube was bent at RT, which shows that cryogenic bending can effectively avoid fracture. As the temperature decreases, however, the improvement of tube formability is not monotonic, and the degree of wrinkling decreases first and then increases. The average and maximum wrinkle heights both decrease first and then increase with the temperature decreasing. But for the thinning of wall thickness, it decreases continuously with the temperature getting lower.

The influence of temperature on each defect were analyzed and compared to determine the optimum bending temperature. The minimum degree of wrinkling appeared at -60°C and the wrinkling degree is very low which can be considered almost has no wrinkle and there is only a wrinkling tendency. On the other hand, the temperature for maximum avoiding wall thickness reduction is -180°C. However, it can be found that Δt decreases most rapidly as the temperature decreasing from RT to -60°C. The average Δt has been reduced about 23.7% from RT to below 0.15 at -60°C, which

shows that the forming quality is significantly improved. When the temperature continues to decrease, the improvement of the wall thickness reduction is no longer obvious. Due to the consideration of the effect of cryogenic temperature on forming defects and the cost of cryogenic bending tests, -60℃ was finally selected as the most optimum temperature for bending of LDTW Al-alloy tubes.

- *Breaking bending limits by cryogenic forming*

To further explore the bending limit at CT, numerical simulations of tube bending with different bending radii were carried out by cryogenic forming. The bending radius was set as 1.5*D*, 1.0*D* and 0.8*D*, and the tube formability with R_d=2.0*D* was taken to make comparison. Forming temperature is set as the most optimum temperature -60°C. Fig. 21 and Table 10 show the results of rotary draw bending of LDTW 6061-O Al-alloy tubes at different bending radii at -60°C. It indicates that the degree of forming defects increases as the bending radius decreases. When the bending radius reaches 0.8*D*, the tube cannot complete the bending due to a crack.

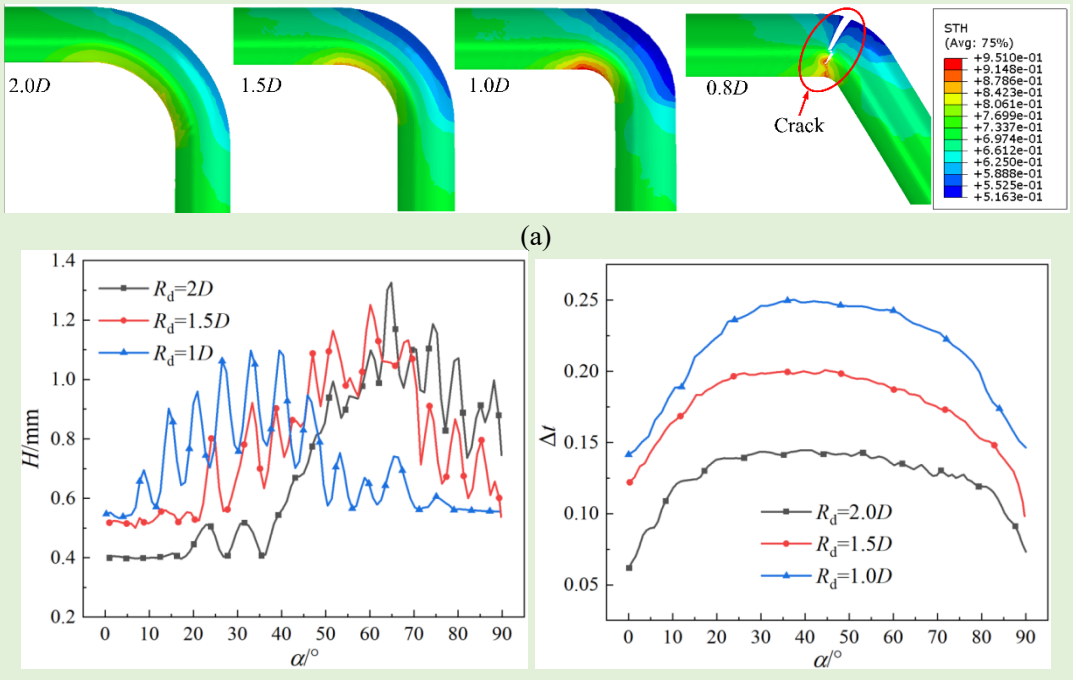

Fig. 21. Results of rotary draw bending of LDTW 6061-O Al-alloy tubes with different bending radii at -60°C: (a) overview of simulation results, (b) wrinkling pattern along tube inner ridgeline, (c) wall thickness reduction rate along tube outer ridgeline.

Table 10. Forming defects at different bending radii.

bending radius	Number of $\Delta H >$ 0.35 mm	Average ΔH /mm	Maximum ΔH /mm	Average Δt	Maximum Δt
2.0*D*	0	0.22	0.35	0.125	0.144
1.5*D*	0	0.24	0.35	0.175	0.201
1.0*D*	0	0.27	0.36	0.224	0.250

For the results of wrinkling, both average ΔH and maximum ΔH become larger as

the bending radius getting small. In addition, the wrinkling tendency trends to appear later as the bending radius getting lower. When the bending radius is 2.0D, wrinkling tendency is mainly concentrated at the front end of the tube while that occurs at the rear end when the bending radius is reduced to 1.0D. While there is no wrinkle wave with $\Delta H > 0.35$ mm occurs, a critical maximum ΔH of 0.35 mm occurs when the bending radius reduces to 1.0D, which means that the bending limit at which wrinkling does not occur has been reached.

The wall thickness reduction rate Δt increases significantly as the bending radius decreases from 2.0D to 1.0D. When the bending radius is 1.0D, the maximum Δt has reached 0.260, which is a very critical state for such LDTW 6061-O Al-alloy tubes, and finally cracks when the bending radius reduces to 0.8D. So, the bending limit within the thinning range that the tube wall can withstand is also 1.0D. Therefore, for the LDTW 6061-O Al-alloy tubes (D/t=89) studied in this work, the theoretically achievable bending limit is 1.0D bending radius.

5.3 Inhibition mechanism of cryogenic temperature on forming defects

Many research attributed the formability development in Al-alloy component to cryogenic enhancement in the tensile strength and ductility of Al-alloy materials, which are related to dynamic recovery [40], dislocation type transition [41], and second phase interaction [42],[43]. But for cryogenic bending, the improvement of tube formability is the result of the comprehensive superposition of the influence by these material mechanical properties and tools constraints related friction behavior, rather than simple improving as the temperature decreasing. Accordingly, the effects of cryogenic temperature on tube bending formability are mainly affected by two aspects, one is the overall improvement of the mechanical properties of Al-alloy tubes at CT, and the other is the effect of the change of friction coefficient between tube and tooling dies at CT. Inhibition mechanisms of cryogenic temperature on forming defects are analyzed from the corresponding two aspects.

Mechanical properties involving fracture energy C, anisotropy index r, strength factor K and hardening index n and friction coefficients between tube and bending die, mandrel die, pressure die and wiper die were taken to study the effect of CT on Δt and ΔH, respectively. According to the results obtained in Section 5.2, bending radius is set as 2.0D. A method of controlling for a single variable was employed, and the parameter ranges for each set of variables correspond to the parameter ranges at the studied temperatures. For other parameter settings except variables, they are consistent with the condition under bending at RT for the study of variables C, r and n. Since cracks may occur for the study of variables that may enhance bending defects at CT, viz. K and friction coefficients, when the other parameter settings are same as the condition at RT, thus the condition at -60℃ is selected for the study of these variables.

- *Effect of cryogenic temperature on wall thinning and cracking*

The results of the effects of CT on wall thinning and cracking were obtained in Fig. 22. It can be seen from the figure that the influences of different variables on the wall thickness reduction are quite different. Variations of mechanical properties at CT have

a greater effect on Δt than those of frictional properties.

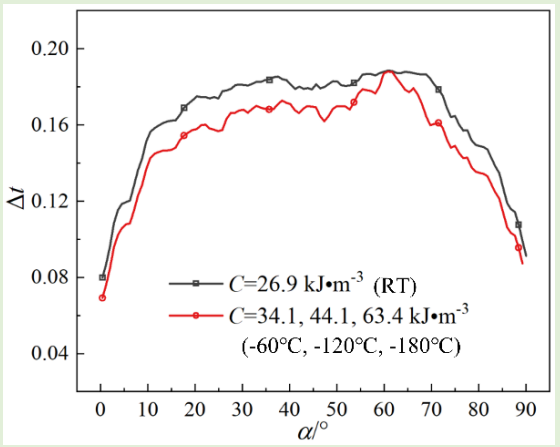

(a)

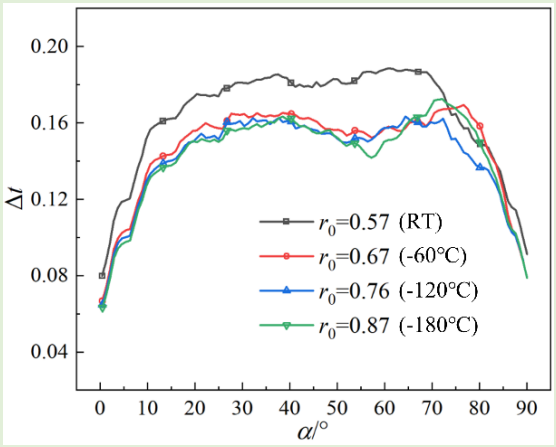

(b)

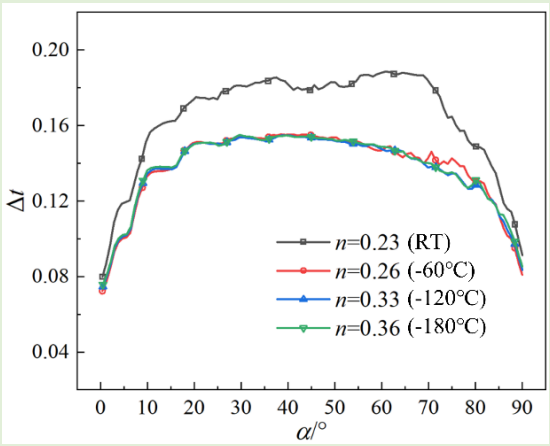

(c)

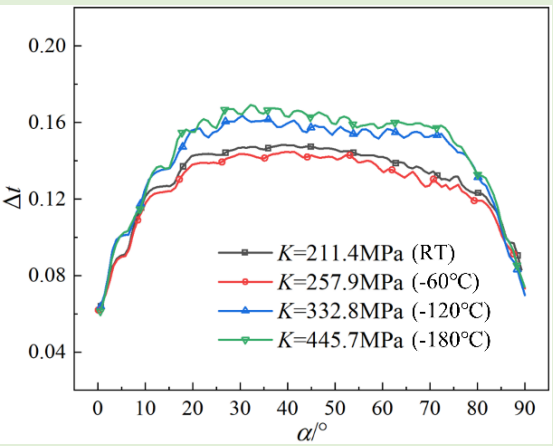

(d)

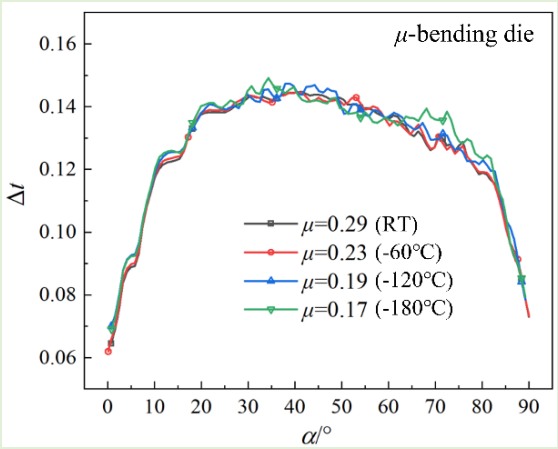

(e)

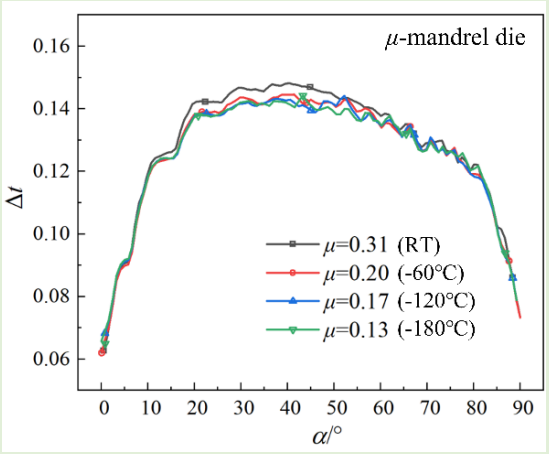

(f)

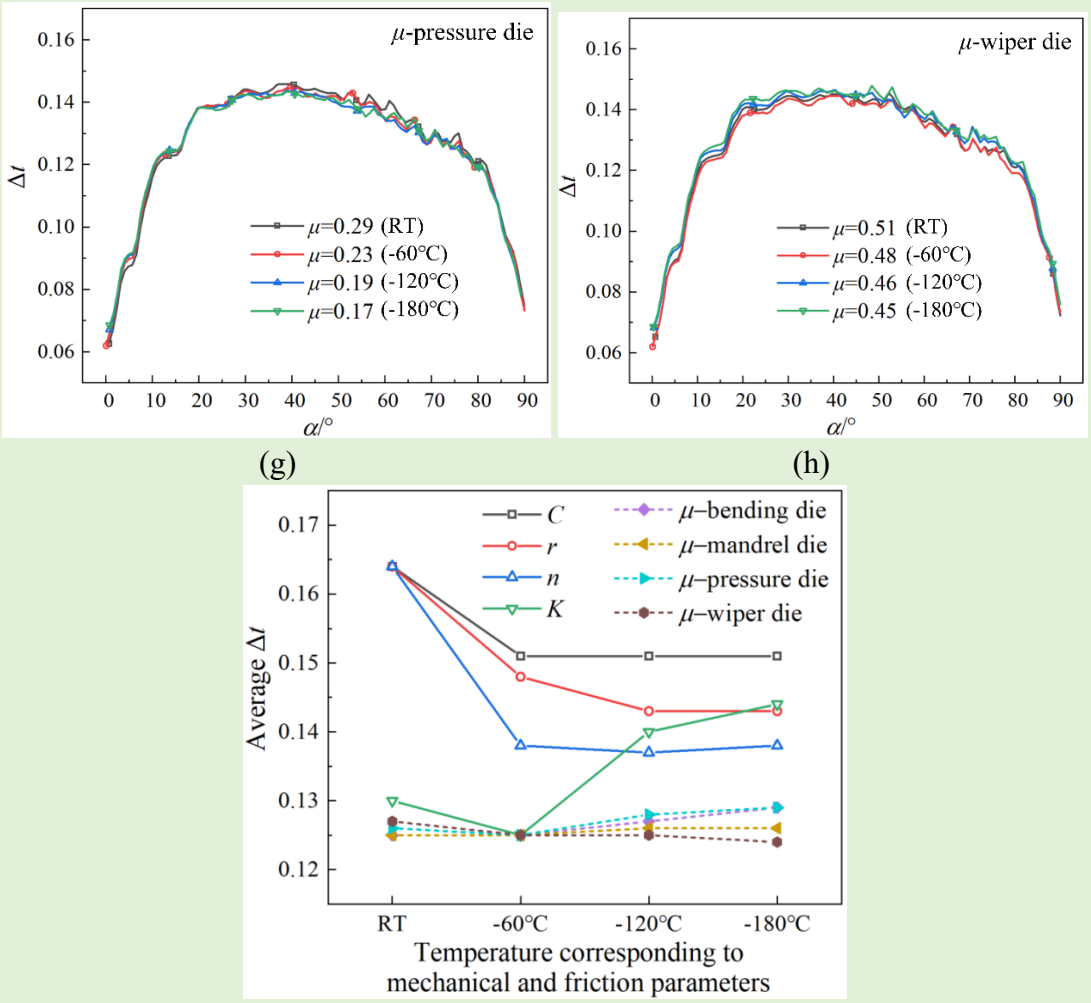

Fig. 19. Effects of mechanical properties and friction coefficients under different temperatures on Δt with 2D bending radius: (a) C, (b) r, (c) n, (d) K, and friction coefficients between tube and (e) bending die, (f) mandrel die, (g) pressure die and (h) wiper die and (i) the trend of average Δt under different temperatures corresponding to variables change.

Mechanical properties of C, r, n and K all increase with the decrease of temperature, and the cryogenic enhancement of C, r and n can reduce wall thinning of tube, conversely, a larger K at CT intensifies wall thinning.

For the effect of the variable fracture energy C, when the temperature drops from RT to -60°C, the average Δt decreases by about 8%, and the maximum Δt remains basically unchanged. As the temperature continues to drop, the wall thinning no longer changes with temperature. This is because the elongation of the material increases significantly at CT, and accordingly the fracture energy increases. When the fracture energy of the material is greater than the threshold fracture energy, the change of C value has little effect on the material defects. For the effect of the variable r-value, the wall thinning is significantly weakened with the decrease of temperature, especially when the temperature is reduced from RT to -60°C, the average Δt is decreased by about 10%. The effect of the variable n values is very similar of that of the variable r-value, and somewhat more drastically. The average Δt decreased by about 16% at -60°C and then

remained stable. When K increases, the average Δt first decreases slightly (about 4%) at -60°C, then increases as the temperature getting lower, and increases by about 11% at -180°C. The influences of the above four mechanical properties on wall thinning at CT can well explain why Δt decreases at CT and drops most fast from RT to -60°C.

From the perspective of material deformation mechanism, the cryogenic effect of material properties on wall thickness reduction can be explained from two aspects. One is that the strength and hardening of the material are improved at CT, accompanied with a lager elongation, results in enhancements of C, n and K at CT. Thus, the proportion of uniform plastic deformation stage in the entire deformation process will increase accordingly, thereby reducing wall thinning. Another is that the increased anisotropy index r-value under CT also promotes a more uniform deformation. The tube outer ridge is mainly subjected to tensile stress. When r is less than 1, according to the definition of Eq. (1), the shrinkage strain of the material in the transverse direction is smaller than that in the thickness direction. As the temperature decreases, the r-value increases significantly and is closer to 1. This means that the material is less anisotropic at CT and its shrinkage strain is more uniform in the transverse and thickness directions. In other words, the cryogenic environment can weaken the anisotropy of LDTW Al-alloy tubes, thereby effectively reducing wall thinning and cracking during forming. Fig. 23 shows the fracture sections of the specimens after uniaxial tensile fracturing at RT and -180℃. While the elongation is greatly improved at -180℃, the aspect ratio of fracture cross-section is more uniform, and the thickness shrinkage is not as strong as it at RT. This can also intuitively explain the decrease in tube wall thinning at CT.

For the effects of restraint, tube wall thinning at CT is mainly intensified by the friction between tube and pressure die, mandrel die and bending die, offering axial thrust force and inner radial support. According to the cryogenic friction results, when the friction coefficient between tube and pressure die decreases at CT, the thrust force of pressure die and bending die on the tube will decrease accordingly, which is not conducive to reducing Δt. When it is reduced to a certain extent, the tube may even slip from the tooling dies. While Δt is reduced very slightly by the friction between tube and wiper die at CT. This is because the wiper die and the pressure die jointly provide external constraints on the tube, however, the wiper mainly provides support for the inner side of the tube, so it has little impact on the outer thinning. On the whole, the decreasing in friction at CT may increase wall thinning of tubes, but only to a small extent.

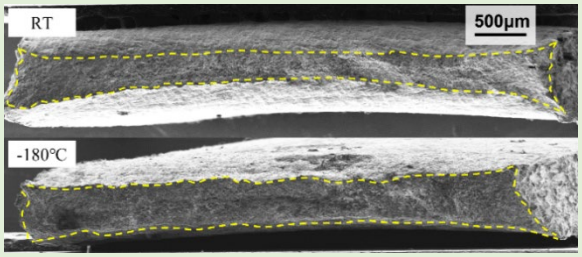

Fig. 23. The fracture sections of the specimens after uniaxial tensile fracturing at RT and -180℃.

- *Effect of cryogenic temperature on wrinkling*

Compared with the sheet forming, tubes have the characteristics of circumferential

closure, which makes it have geometric self-constraints, thus the instability problem during forming process of tubes is more complicated [44]. From the results in Section 5.2, the effect of temperature on wrinkling is not monotonous. Instead, as the temperature decreases, it first decreases and then increases. The lowest degree of wrinkling occurs when bending at -60°C. The reason is that not all enhancements of material properties and decreasing in friction at CT are beneficial to suppress wrinkling. The results of the effects of CT on wrinkling were obtained in Fig. 24.

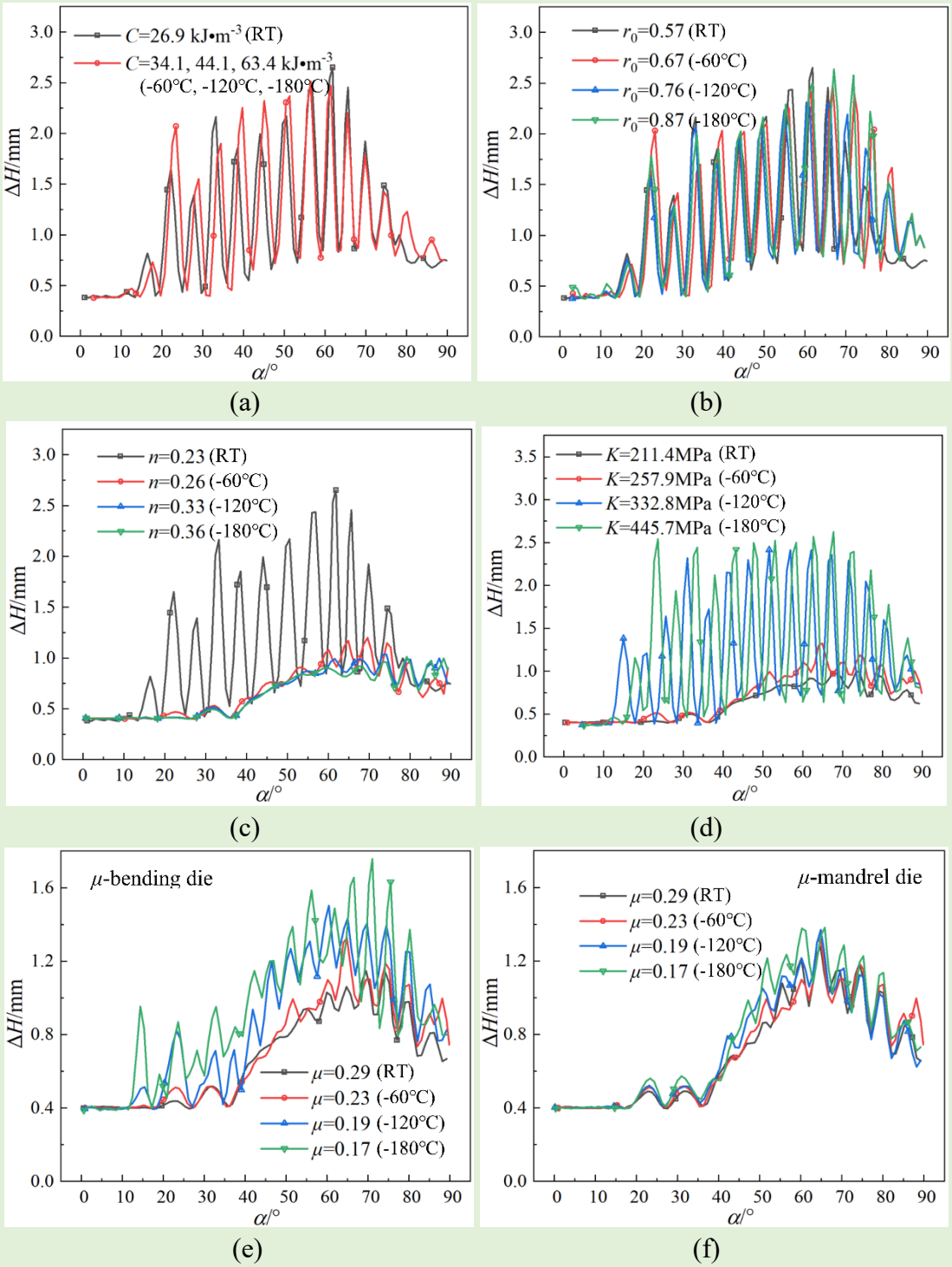

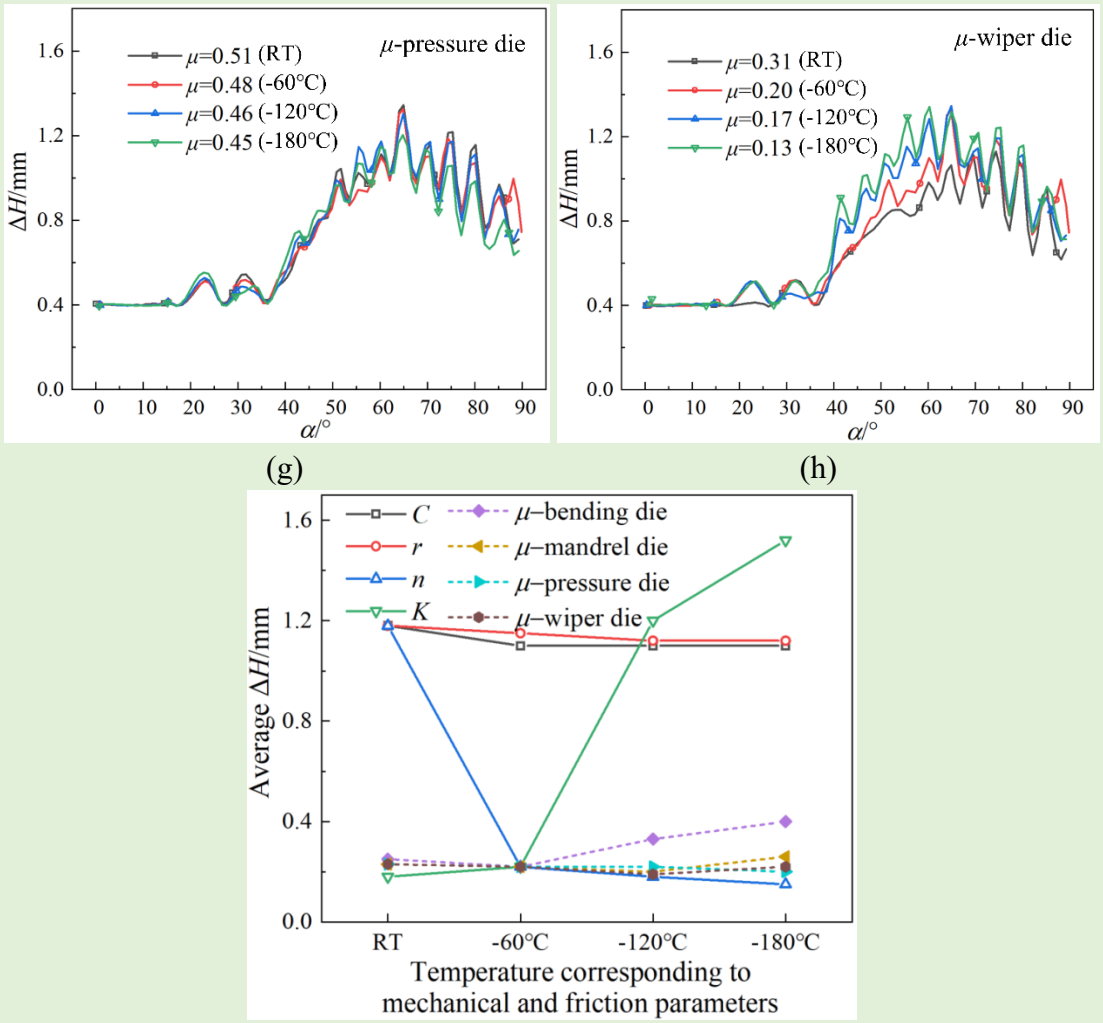

Fig. 24. Effects of mechanical properties and friction coefficients under different temperatures on ΔH with $2D$ bending radius: (a) C, (b) r, (c) n, (d) K, and friction coefficients between tube and (e) bending die, (f) mandrel die, (g) pressure die and (h) wiper die and (i) the trend of average ΔH under different temperatures corresponding to variables change.

It can be found that the most significant impacts on wrinkling at CT is owing to the mechanical properties n and K, and the influence of the two factors on wrinkling varies with temperature in the opposite direction, which directly leads to the non-monotonic variation of wrinkling with temperature. Mathematically, the hardening index n is the power exponent of the Swift hardening law fitting stress-strain curve in the plastic deformation stage, which can reflect the uniformity of plastic deformation. The increase of the n value makes the deformation more uniform, leading to a reduction of the compressive stress on the tube inner ridge, so that wrinkling is more difficult to occur. On the contrary, an increase in strength factor K is not conducive to suppressing tube wrinkling [45] due to the fact that the compressive stress applied on tube inner ridge raises during the bending process with the increase of K, which promotes wrinkling degree accordingly [46]. The effects of C and r-value also tend to reduce wrinkling for a fracture energy above the threshold and more uniform strain distribution during deformation, but the degrees are not obvious.

In addition, influence of friction at CT on wrinkling should also be considered. The friction force of the wiper die, pressure die as well as mandrel on the tube can increase the tangential compressive stress at tube inner ridge. When the friction coefficients decrease at CT, the friction force decreases accordingly, which helps to weaken the tendency and degree of wrinkling. But on the other hand, when the friction force of bending die on the tube is reduced at CT, it leads to accelerate wrinkling for less support force generated by bending die.

In general, the impacts of different variables on wrinkling are different and diverse from those on tube wall thinning, with some properties inhibiting wrinkling and others promoting it. The non-monotonic relationship between wrinkling degree and CT is a result of interactions among multiple factors.

5.4 Experimental verification for tube formability improvement by cryogenic forming

Cryogenic forming of LDTW Al-alloy tubes with R_d=2.0D was finally experimentally performed by the designed cryogenic bending platform. Forming temperature was set as the most optimum temperature -60℃. Fig. 25 shows the tube samples bent at RT and -60℃, respectively. Compared with the tube bent at RT, the forming quality of the tube by cryogenic bending at -60℃ shown in Fig. 25 (b) is significantly improved, no crack and no wrinkle appears on tube inner ridge. The results of cryogenic bending successfully verified the effect of cryogenic temperature on developing formability of LDTW Al-alloy tubes. It is a great improvement for avoiding wrinkling and wall thinning for bending of LDTW 6061-O Al-alloy tubes by cryogenic forming.

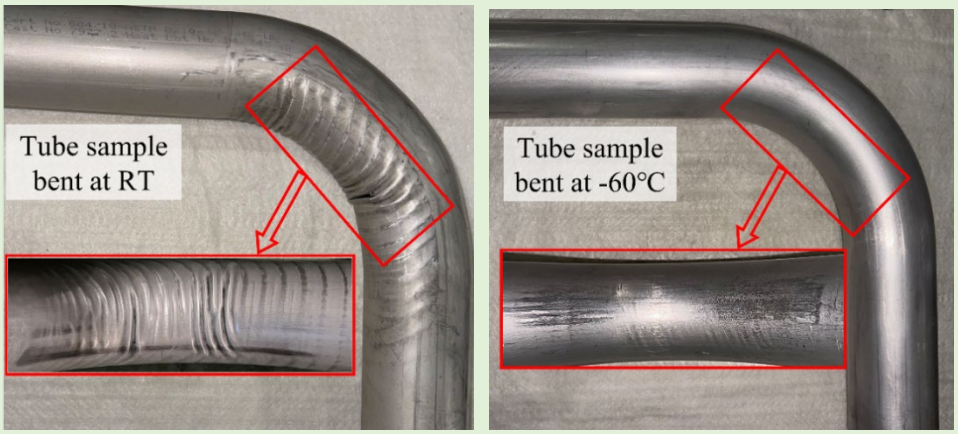

(a) (b)

Fig. 25. Experiment result of rotary draw bending of LDTW 6061-O Al-alloy tubes with 2.0D bending radius: (a) at RT, (b) at -60℃.

6 Conclusions

In this study, cryogenic forming of Al-alloy materials is used to effectively solve the tough issue of precise bending of the hard-to-form tubular materials with extremely specification. Here are the main conclusions.

(1) Cryogenic characterizations of LDTW Al-alloy tubes, including material mechanical properties and friction behaviors, have been realized. A characterization

method by combining experiment and VPSC-based simulation was investigated to solve the anisotropic parameters at CT. As the temperature decreases, the mechanical properties of the LDTW 6061-O Al-alloy tubes are significantly improved, and the friction coefficients exhibit varying degrees of decline.

(2) An innovative cryogenic bending method was investigated and the experiment platform of tube rotary draw bending at cryogenic temperature was well designed. Internal and external cooling channels was approached to realize tube cooling during the whole bending process. The cooling efficiency was compared and optimized, it is very necessary to cool down the tube by dual cooling of inner and outer channels.

(3) It is proved that tube formability evaluated by two bending defects of wall thinning and wrinkling can be effectively improved by cryogenic bending. As the temperature decreases, tube thickness reduction decreases continuously, however, the degree of wrinkling decreases first and then increases, and the most optimum temperature was obtained at -60℃. Bending limit has been further explored and it has been improved from R_d=3.0D at RT to 1.0D at -60℃. Cryogenic bending of LDTW Al-alloy tubes with R_d=2.0D at -60℃ was finally experimentally performed.

(4) For wall thickness reduction, cryogenic enhancement of C, r and n can reduce it, conversely, a larger K at CT intensifies it. The decreasing in friction of wiper die and pressure die at CT can promote wall thinning but only to a very small extent. For wrinkling, the opposite effects of strength factor K and hardening index n mainly cause of the non-monotonic relation between the temperature and wrinkling degree. The friction of bending die also has an impact to increase wrinkling at CT.

Acknowledgement

The authors would gratefully acknowledge the support from the National Science Fund for Excellent Young Scholars (51522509). Hong Sun would like to thank the funding support under the project of SB3Q from The Hong Kong Polytechnic University for joint-supervision of PhD study.

References

[1] J. Ma, T. Welo, D. Wan, The impact of thermo-mechanical processing routes on product quality in integrated aluminium tube bending process, Journal of Manufacturing Processes 67 (2021) 503-512. https://doi.org/10.1016/j.jmapro.2021.05.015

[2] H. Yang, H. Li, J. Ma, G. Li, D. Huang, Breaking bending limit of difficult-to-form titanium tubes by differential heating-based reconstruction of neutral layer shifting, International Journal of Machine Tools and Manufacture, 166 (2021) 103742. https://doi.org/10.1016/j.ijmachtools.2021.103742

[3] H. Sun, H. Li, F. Gong, Y. Liu, G. Li, M.W. Fu. Filler parameters affected wrinkling behavior of aluminum alloy double-layered gap tube in rotary draw bending process. The International Journal of Advanced Manufacturing Technology, 119 (2022) 5261-5276. https://doi.org/10.1007/s00170-021-08375-7

[4] Li H, Yang H, Zhang Z, Wang Z. 'Size effect' related bending formability of thin-walled aluminum alloy tube. Chinese Journal of Aeronautics 2013; 26:230-241. https://doi.org/10.1016/j.cja.2012.12.025

[5] Yang H, Li H, Zhang Z, Zhan M, Liu J, Li G. Advances and Trends on Tube Bending Forming Technologies. Chinese Journal of Aeronautics 2012; 25:1-12. https://doi.org/10.1016/S1000-9361(11)60356-7

[6] H. Li, H. Yang, Z.Y. Zhang, G.J. Li, N. Liu, T. Welo, Multiple instability-constrained tube bending limits, Journal of Materials Processing Technology, 214 (2014) 2 445-455. https://doi.org/10.1016/j.jmatprotec.2013.09.027

[7] Y.X. Zhu, Y.L. Liu, H.P. Li, H. Yang, Comparison between the effects of PVC mandrel and mandrel-cores die on the forming quality of bending rectangular H96 tube. International Journal of Mechanical Sciences 2013; 76: 132-143. https://doi.org/10.1016/j.ijmecsci.2013.09.011

[8] C. Liu, Y. Liu, Cross-sectional deformation behavior of double-ridged rectangular tube with fillers in different stages of H-typed bending. Chinese Journal of Aeronautics 2020; 33: 1799-1811. https://doi.org/10.1016/j.cja.2019.08.005

[9] Z.Y. Zhang, H. Yang, H. Li, N. Ren, D. Wang, Quasi-static tensile behavior and constitutive modeling of large diameter thin-walled commercial pure titanium tube, Materials Science and Engineering: A, 569 (2013) 96-105. https://doi.org/10.1016/j.msea.2013.01.055

[10] J. Ma, H. Li, D. Wang, M.W. Fu, Z.J. Tao, Tribological behaviors in titanium sheet and tube forming at elevated temperatures: evaluation and modeling, Int. J. Adv. Manuf. Technol. 97 (2018) 657–674, https://doi.org/10.1007/s00170-018-1985-y.

[11] X.L. Zhang, H. Yang, H. Li, Z.Y. Zhang, L. Li, Warm bending mechanism of extrados and intrados of large diameter thin-walled CP-Ti tubes. Transactions of Nonferrous Metals Society of China 2014; 24 (10): 3257-3264. https://doi.org/10.1016/S1003-6326(14)63465-8

[12] Zhi-jun TAO, Xiao-guang FAN, He YANG, Jun MA, Heng LI, A modified Johnson–Cook model for NC warm bending of large diameter thin-walled Ti–6Al–4V tube in wide ranges of strain rates and temperatures. Transactions of Nonferrous Metals Society of China 2018; 28 (2): 298-308. https://doi.org/10.1016/S1003-6326(18)64663-1

[13] Enrico Simonetto, Andrea Ghiotti, Stefania Bruschi, High accuracy direct hot bending of hollow profiles. Manufacturing Letters 2021; 27: 63-66. https://doi.org/10.1016/j.mfglet.2020.12.005

[14] Sonia P, Verma V, Saxena KK, Kishore N, Rana R S. Effect of cryogenic treatment on mechanical properties and microstructure of aluminium 6082 alloy. Materials Today: Proceedings 2020; 26:2248-2253. https://doi.org/10.1016/j.matpr.2020.02.488

[15] Cheng W, Liu W, Fan X, Yuan S. Cooperative enhancements in ductility and strain hardening of a solution-treated Al-Cu-Mn alloy at cryogenic temperatures. Materials Science and Engineering: A 2020; 790:139707. https://doi.org/10.1016/j.msea.2020.139707

[16] Xiaobo Fan, Xianshuo Chen, Shijian Yuan, Novel forming process for aluminum alloy thin shells at ultra-low temperature gradient, International Journal of Machine Tools and Manufacture, 185 (2023) 103992. https://doi.org/10.1016/j.ijmachtools.2022.103992

[17] Yuan S, Cheng W, Liu W, Xu Y. A novel deep drawing process for aluminum alloy sheets at cryogenic temperatures. Journal of Materials Processing Technology 2020; 284:116743. https://doi.org/10.1016/j.jmatprotec.2020.116743

[18] Schneider R, Heine B, Grant RJ, Zouaoui Z. Aluminium sheet metal forming at low temperatures. IOP Conference Series: Materials Science and Engineering 2015; 74:012014.

[19] Liu W, Cheng W, Yuan S. Analyses on formability and flow stress of an Al-Cu-Mn alloy sheet under biaxial stress at cryogenic temperatures. International Journal of Mechanical Sciences 2021; 195:106266. https://doi.org/10.1016/j.ijmecsci.2021.106266

[20] Sotirov N, Falkinger G, Grabner F, Schmid G, Schneider R, Grant RJ, Kelsch R, Radlmayr K, Scheerer M, Reichl C, Sehrschön H, Loipetsberger M. Improved formability of AA5182 aluminium alloy sheet at cryogenic temperatures.

Materials Today: Proceedings 2015; 2:S113-S118. https://doi.org/10.1016/j.matpr.2015.05.027

[21] Araghchi M, Mansouri H, Vafaei R, Guo Y. A novel cryogenic treatment for reduction of residual stresses in 2024 aluminum alloy. Materials Science and Engineering: A 2017; 689:48-52. https://doi.org/10.1016/j.msea.2017.01.095

[22] Tekkaya AE, Homberg W, Brosius A, eds. 60 Excellent Inventions in Metal Forming. 1st ed. Springer Vieweg; 2015. https://doi.org/10.1007/978-3-662-46312-3

[23] T. Wang, F. Guo, K. Matsuda, Y. Zou, An investigation of cryogenic-aging process attemptted to alleviate mechanical anisotropy of 7055 thick plate, Mater. Sci. Eng. A. (2021) 142589. https://doi.org/10.1016/j.msea.2021.142589

[24] Kuwabara T, Hashimoto K, Iizuka E, Yoon JW. Effect of anisotropic yield functions on the accuracy of hole expansion simulations. Journal of Materials Processing Technology 2011; 211:475-481. https://doi.org/10.1016/j.jmatprotec.2010.10.025

[25] Korkolis YP, Kyriakides S. Inflation and burst of anisotropic aluminum tubes for hydroforming applications. International Journal of Plasticity 2008; 24:509-543. https://doi.org/10.1016/j.ijplas.2007.07.010

[26] Yang H, Li H, Ma J, Wei D, Chen J, Fu MW. Temperature dependent evolution of anisotropy and asymmetry of α-Ti in thermomechanical working: Characterization and modeling. International Journal of Plasticity 2020; 127:102650. https://doi.org/10.1016/j.ijplas.2019.102650

[27] Chan WL, Fu MW, Lu J, Chan LC. Simulation-enabled study of folding defect formation and avoidance in axisymmetrical flanged components. Journal of Materials Processing Technology 2009; 209:5077-5086. https://doi.org/10.1016/j.jmatprotec.2009.02.005

[28] Li H, Yang H, Zhan M, Gu RJ. A new method to accurately obtain wrinkling limit diagram in NC bending process of thin-walled tube with large diameter under different loading paths. Journal of Materials Processing Technology 2006; 177: 192-196. https://doi.org/10.1016/j.jmatprotec.2006.03.191

[29] Gao Y, Li H, Zhao D, Wang M, Fan X. Cryogenic friction behavior of aluminum alloys sheets under dry contact condition. Tribology International 2023; 180:108227. https://doi.org/10.1016/j.triboint.2023.108227

[30] Hong Sun, Heng Li, Lihui Yi, Yuli Liu, Juan Du, M.W. Fu. Prediction and control of bending quality of double-layered gap tube, International Journal of Mechanical Sciences, 2022, 228, 107474. https://doi.org/10.1016/j.ijmecsci.2022.107474.

[31] Tomé CN, Canova GR, Kocks UF, Christodoulou N, Jonas JJ. The relation between macroscopic and microscopic strain hardening in F.C.C. polycrystals. Acta Metallurgica 1984; 32:1637-1653. https://doi.org/10.1016/0001-6160(84)90222-0

[32] Tomé CN, Lebensohn RA, 2009. Manual for Code Visco-Plastic Self-Consistent. Los Alamos Natl. Lab, USA. https://www.scribd.com/document/395219950/VPSC7c-Manual

[33] Yang H, Li H, Ma J, Zhang Z, Chen J. Constitutive modeling related uncertainties: Effects on deformation prediction accuracy of sheet metallic materials. International Journal of Mechanical Sciences 2019; 157-158:574-598. https://doi.org/10.1016/j.ijmecsci.2019.05.004

[34] Hill R. A theory of the yielding and plastic flow of anisotropic metals. Proceedings of the Royal Society of London. Series A. Mathematical and Physical Sciences 1948; 193:281-297. https://doi.org/10.1098/rspa.1948.0045

[35] Barlat F, Brem JC, Yoon JW, Chung K, Dick RE, Lege DJ, Pourboghrat F, Choi SH, Chu E. Plane stress yield function for aluminum alloy sheets-part 1: theory. International Journal of Plasticity 2003; 19:1297-1319. https://doi.org/10.1016/S0749-6419(02)00019-0

[36] Hershey AV. The plasticity of an isotropic aggregate of anisotropic face centred cubic crystals. Journal of Applied Mechanics 1954; 21:241-249. https://doi.org/10.1115/1.4010900

[37] Hosford WF. A generalized isotropic yield criterion. Journal of Applied Mechanics 1972; 39:607-609. https://doi.org/10.1115/1.3422732

[38] Z. Xue, M.G. Pontin, F.W. Zok, J.W. Hutchinson, Calibration procedures for a computational model of ductile fracture, Eng. Fract. Mech. 77 (2010) 492-509.

[39] T. Wierzbicki, Y. Bao, Y.W. Lee, Y. Bai, Calibration and evaluation of seven fracture models, Int. J. Mech. Sci. 47 (2005) 719-743.

[40] B.B. Rath, C.S. Pande, Recovery of low-temperature flow stress in zone-refined aluminum single crystals, Acta Materialia. 61 (2013) 3735-3743. https://doi.org/10.1016/j.actamat.2013.02.056

[41] B. Gruber, I. Weiensteiner, T. Kremmer, F. Grabner, G. Falkinger, A. Schökel, F. Spieckermann, R. Schäublin, P.J. Uggowitzer, S. Pogatscher, Mechanism of low temperature deformation in aluminium alloys, Mater. Sci. Eng. A. 795 (2020) 139935. https://doi.org/10.1016/j.msea.2020.139935

[42] K. Huang, S. Huang, Y. Yi, F. Dong, H. He. Flow behavior and forming characteristic of 2A14 aluminum alloy at cryogenic temperature. J. Alloys Compd. (2022) 163821. https://doi.org/10.1016/j.jallcom.2022.163821

[43] D.C.C. Magalhães, A.M. Kliauga, M.F. Hupalo, O.M. Cintho, C.A.D. Rovere, M. Ferrante, V.L. Sordi, The influence of Cryo-ECAP and aging on the microstructure and mechanical behavior of AA6061 Al alloy, Mater. Sci. Eng. A. 768 (2019) 138485. https://doi.org/10.1016/j.msea.2019.138485

[44] Heng Li, Hong Sun, Haoran Liu, Nan Liu. Loading conditions constrained wrinkling behaviors of thin-walled sheet/tube parts during metal forming. Journal of Materials Processing Technology, 296(2021): 117199.

[45] A.M. Szacinski, P.F. Thomson, The effect of mechanical properties on the wrinkling behaviour of sheet materials in the yoshida test, Journal of Mechanical Working Technology, 10 (1984) 1: 87-102. https://doi.org/10.1016/0378-3804(84)90081-0

[46] He Yang, Yan Lin, Wrinkling analysis for forming limit of tube bending processes, Journal of Materials Processing Technology 152 (2004) 363-369. https://doi.org/10.1016/j.jmatprotec.2004.04.410